Chapter 1

Introduction and Literature Review

1.1 Hall effect: historical background and development

1.1.1 Ordinary Hall effect

In 1879, Edwin H. Hall discovered that when a current-carrying conductor is placed in a perpendicular magnetic field [Fig. 1.1], the Lorentz force acting on charge carriers gives rise to a voltage, transverse to both the current (j) and the magnetic field (H) [1].

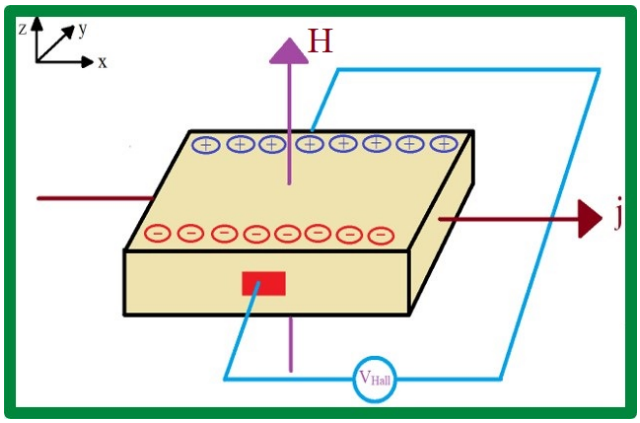

Figure 1.1: Schematic for the measurement of the Hall effect.

The transverse resistivity/Hall resistivity (ρ_{xy}) corresponding to the transverse voltage is found to be directly related to the applied magnetic field through the relation $\rho_{xy} = R_O$H, as depicted in Fig. 1.2 (a), where $R_O = \frac{1}{ne}$ is known as the ordinary Hall coefficient, n is the charge carrier density, and e is the electron charge. The sign and magnitude of the ordinary Hall coefficient give information about the type of charge carriers (electron or hole) and the concentration of charge carriers, respectively, present in the conductor. This transverse transport phenomenon, which is explained classically, is known as the ordinary Hall effect (OHE) and is well understood. The discovery of OHE introduced a simple and elegant device for measuring carrier concentration in nonmagnetic conductors, which significantly contributed to semiconductor physics and the emergence of solid-state electronics in the late 1940s.

1.1.2 Anomalous Hall effect

After two years, in 1881, Edwin H. Hall made the historic discovery that the Hall effect is ten times larger in ferromagnetic conductors such as Fe, Ni, Co, which is related to its property of broken time-

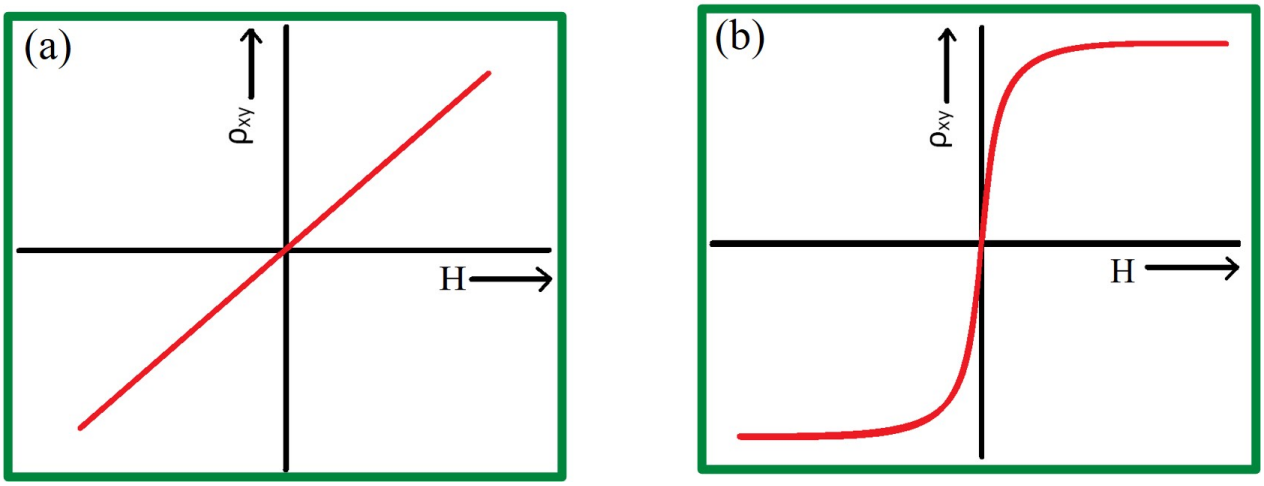

Figure 1.2: Typical behaviors of the ordinary Hall and anomalous Hall effects. The Hall resistivity ρ_{xy} is plotted versus external magnetic field H. (a) Ordinary Hall effect; (b) Anomalous Hall effect.

reversal symmetry as compared to nonmagnetic conductors [2]. This phenomenon is known as the anomalous Hall effect (AHE), and the anomalous contribution is often observed to be proportional to the magnetization (M), as shown in Fig. 1.2 (b). After that, numerous experiments established an empirical relationship among ρ_{xy}, H, and M [3]-

$$\rho_{xy} = R_O H + R_S M \tag{1.1}$$

The second term represents the anomalous Hall contribution in ρ_{xy}. The coefficient R_S is the anomalous Hall coefficient, which depends on the material-specific property, particularly on longitudinal resistivity (ρ_{xx}) [3]. The AHE was discovered more than a century ago, attained a vast interest in current years due to its role in understanding the fundamental physics [3, 4, 5, 6, 7, 8, 21] and potential for applications in spintronics-based data storage devices and Hall sensors [10, 11, 12, 13, 14, 15, 16].

1.1.3 Origin of anomalous Hall effect

1.1.3.1 Karplus and Luttinger theory

In 1954, Karplus and Luttinger (KL) proposed a theory for the AHE in which they showed that when an external electric field is applied to solids [Fig. 1.3], charge carriers acquire an additional velocity to their group velocity [17]. This anomalous velocity will be perpendicular to the electric field,

and hence, contribute to the Hall effect. In the case of ferromagnetic solids, the sum of anomalous velocity over the whole occupied band state can be nonzero, giving rise to an anomalous contribution to the Hall conductivity (σ_{xy}). As this contribution purely depends on the electronic band structure in contrast to the scattering of charge carriers, it is known as an intrinsic contribution to the AHE. The anomalous velocity depends only on the perfect crystal Hamiltonian and, therefore, can be related to the change in phase of the Bloch wave function of charge carriers when an electric field induces them to revolve in the crystal momentum space [18, 19].

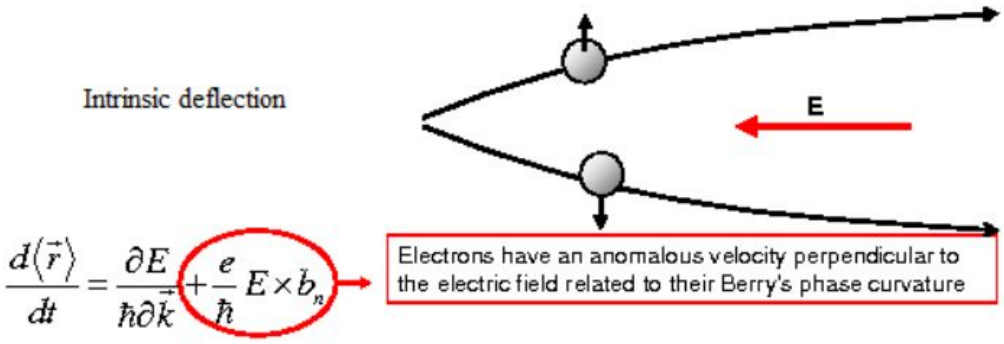

Figure 1.3: Schematic of intrinsic anomalous Hall effect due to the deflection of electrons from the Berry curvature [3].

1.1.3.2 Extrinsic skew scattering mechanism

The main drawback of KL theory is the absence of discussion about disorder-induced scattering in imperfect crystals, which may also contribute to the Hall effect. In 1955, Smit discovered that the asymmetric scattering (skew scattering) of charge carriers [Fig. 1.4 (a)] from magnetic impurities caused by spin-orbit coupling (SOC), may give rise to extrinsic AHE [20]. The extrinsic AHE is purely related to the scattering mechanism. Therefore, the Hall conductivity (σ_{xy}) due to the skew scattering mechanism is proportional to the relaxation time (τ) between two consecutive scatterings ($\sigma_{xy} \propto \tau$, where $\tau \propto 1/\rho_{xx}$). The ρ_{xy} can be expressed as $\frac{\sigma_{xy}}{\sigma_{xx}^2}$, where $\sigma_{xx} = 1/\rho_{xx}$ is longitudinal conductivity, and thus, the ρ_{xy} due to the extrinsic skew scattering is linearly proportional to the ρ_{xx} ($\rho_{xy} \propto \rho_{xx}$) [3]. A large AHE accompanied by the skew scattering from non-magnetic/magnetic impurities has been observed in the AV_3Sb_5 (A = K, Rb, and Cs) topological materials [21, 22].

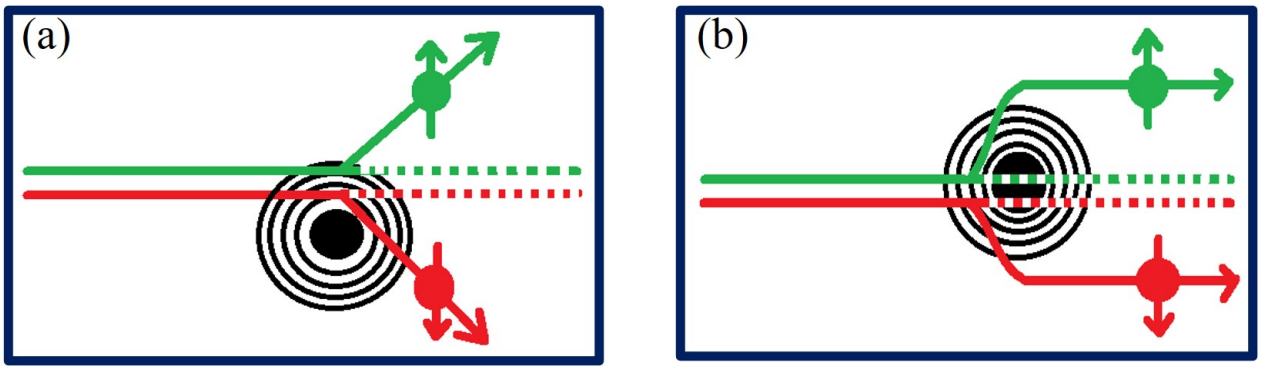

Figure 1.4: Scattering mechanisms responsible for anomalous Hall effect. (a) Skew scattering; (b) Side-jump scattering.

1.1.3.3 Extrinsic side jump mechanism

In 1970, Berger argued that the sudden transverse shift in the propagation direction of charge carriers [Fig. 1.4(b)] from the spin-orbit coupled magnetic impurity may also give rise to extrinsic AHE [23]. The sudden jump results from the combined effect of the SOC and the time delay suffered by the charge carriers, and this delay occurs due to the attractive/repulsive nature of the scattering potential [24]. The side jump-induced extrinsic AHE does not depend on the density of the scatterer and scattering strength. Therefore, σ_{xy} due to the side jump mechanism does not depend on the τ ($\sigma_{xy} \propto \tau^0$), and thus, the $\rho_{xy} = \frac{\sigma_{xy}}{\sigma_{xx}^2}$ due to the extrinsic side jump mechanism will be proportional to the square of the ρ_{xx} ($\rho_{xy} \propto \rho_{xx}^2$) [3]. The AHE plays a crucial role in understanding the low-power dissipation quantum phenomena associated with Berry curvature.

Since the 1980s, the quantum Hall effect (QHE) in two-dimensional (2D) electron systems within semiconductor hetero-structures has emerged as a prominent research field in physics [25]. The hallmark of this phenomenon lies in the precise quantization of Hall conductance [26]. Both the integer effect and fractional QHEs find their explanations in the topological properties (properties remain invariant under small continuous deformation/perturbation) of electronic wave functions. In 2D crystals, Hall conductance is connected to the topological integer (Chern number) (C) [26] [Fig. 1.5], which is defined as the integral of the Bloch state momentum-space Berry curvature over the first-Brillouin zone. This perspective about QHE began influencing the AHE problems around 1998. Theoretical interest in the Berry phase and its connection to transport phenomena, along with advances in complex magnetic systems with strong SOC reignited the AHE research, which leads

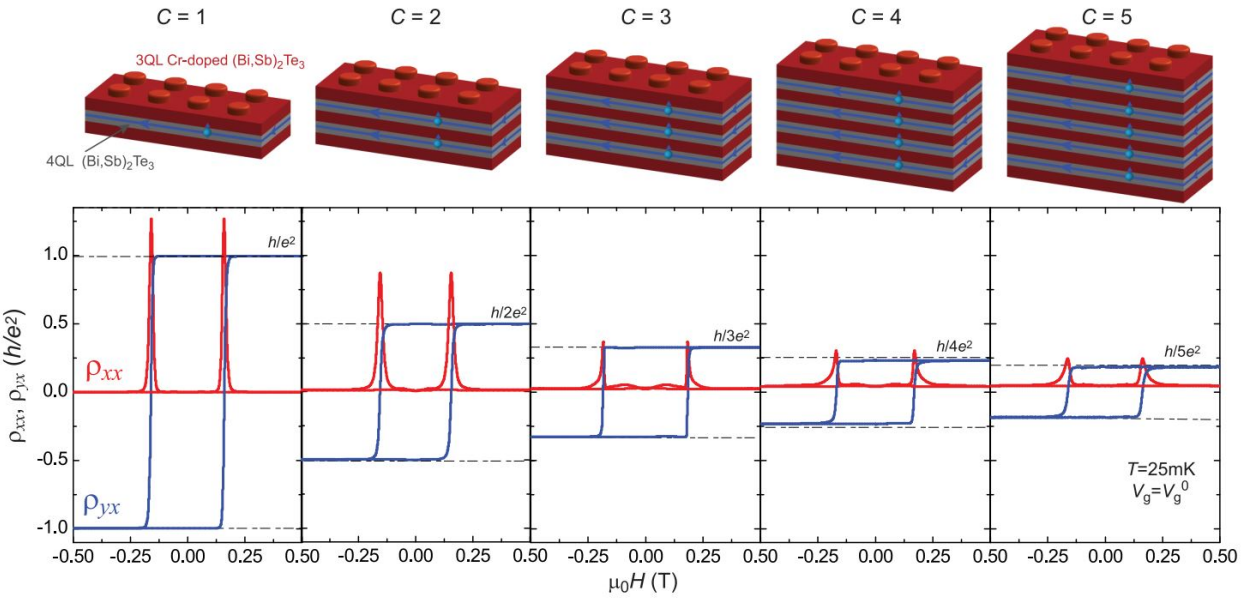

Figure 1.5: Quantum anomalous Hall effect proportional to the Chern number (C) in magnetic topological insulator/topological insulator multi-layer structure [27].

to deeper insights.

1.1.3.4 Intrinsic Berry curvature mechanism

Nowadays, the KL theory is interpreted in terms of the Berry phase and Berry curvature effects in momentum space. In 1984, Michael Berry wrote a theoretical paper about the adiabatic evolution of the eigenstate when external parameters of a quantum system change slowly and make a loop in parametric space [28]. The eigenstate will surely come back to its initial state after traversing the loop, but there will be an evolution of the extra phase, which is commonly known as the Berry phase. The Berry phase is a pure geometrical aspect, which can be written as a line integral of a local geometric quantity over the loop in parametric space. In other words, Berry showed that one could write the Berry phase as an integral of the fictitious magnetic field, which is now called the Berry curvature, over a surface suspending the loop.

In brief, to understand the Berry phase concept in momentum space, let us consider an electron in a periodic potential, and the eigenstate is the Bloch state. The momentum vector **k** (of the nucleus as shown in Fig. 1.6 (a)) is slowly taken around a close loop C, while the electron is assumed to be in the same Bloch state $|n(\mathbf{k})\rangle$ parameterized by **k**. When finishing the loop, the electron eigenstate $|\psi\rangle$ does not return to its initial state $|n(\mathbf{k})\rangle$ and acquires a phase χ called Berry phase [Fig. 1.6 (b)],

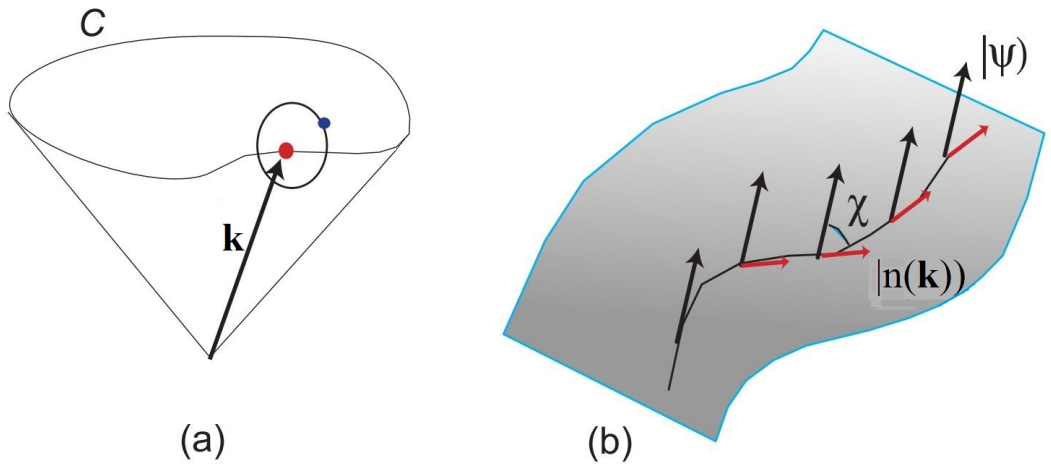

Figure 1.6: (a) Electron constrained to same eigenstate $|n(\mathbf{k})\rangle$ as nuclear coordinate $\mathbf{k}$ is taken around a closed path C. (b) Parallel transport of $|\psi\rangle$ in momentum space. As $\mathbf{k}$ changes, $|\psi\rangle$ acquires a phase angle relative to $|n(\mathbf{k})\rangle$ [29].

viz. $|\psi\rangle = |n(\mathbf{k})\rangle e^{-i\chi}$. Imposing the assumption on the electronic eigenstate, we find [28, 29] -

$$\delta |\psi\rangle = |n(\mathbf{k})\rangle \, e^{-i\chi}(-i\delta\chi)$$

$$\langle n(\mathbf{k})| \, \delta |\psi\rangle = (-i\delta\chi) \, \langle n(\mathbf{k})| \, |n(\mathbf{k})\rangle \, e^{-i\chi}$$

$$\delta\chi = i \, \langle n(\mathbf{k})| \, \delta |n(\mathbf{k})\rangle \tag{1.2}$$

On completing the close curve C, the total Berry phase will be line integral-

$$\chi = \oint_C \langle n(\mathbf{k})| \, i\nabla_{\mathbf{k}} |n(\mathbf{k})\rangle \, d\mathbf{k} \tag{1.3}$$

Physically, as $\mathbf{k}$ changes, there will be a phase angle between the instantaneous electronic ket $|\psi\rangle$ and initial electronic ket $|n(\mathbf{k})\rangle$, which is know as Berry phase/Berry flux. The form of Eq. (1.3) suggests that it is fruitful to view the integrand as a (Berry) vector potential [28]-

$$A_n(\mathbf{k}) = \langle n(\mathbf{k})| \, i\nabla_{\mathbf{k}} |n(\mathbf{k})\rangle \tag{1.4}$$

We may now correlate χ with an Aharanov-Bohm phase caused by a fictitious magnetic field B($\mathbf{k}$) =

$\nabla_{\mathbf{k}} \times \mathrm{A}(\mathbf{k})$, which is also named as Berry curvature $\Omega_n(\mathbf{k})$ in momentum space. The Berry curvature tensor $\Omega^n_{\alpha\beta}$ derived from the Berry vector potential [28]-

$$\Omega^n_{\alpha\beta} = \frac{\delta}{\delta k^\alpha} A^n_\beta - \frac{\delta}{\delta k^\beta} A^n_\alpha$$

$$\Omega^n_{\alpha\beta} = i \left[\langle \frac{\delta n(\mathbf{k})}{\delta k^\alpha} | \, | \frac{\delta n(\mathbf{k})}{\delta k^\beta} \rangle - (\alpha \leftrightarrow \beta) \right] \tag{1.5}$$

The Berry curvature tensor $\Omega^n_{\alpha\beta}$ and vector Ω_n are related by $\Omega^n_{\alpha\beta} = \epsilon_{\alpha\beta\gamma}(\Omega_n)_\gamma$ with $\epsilon_{\alpha\beta\gamma}$ the Levi-Civita anti-symmetric tensor. Besides the differential form in Eq. (1.5), the Berry curvature can be written as the summation over the eigenstates using the Kubo formula approach in the linear response scheme as follows [28]-

$$\Omega^n_{\alpha\beta} = i \sum_{n \neq n'} \frac{\langle n | \frac{\partial H}{\partial k^\alpha} | n' \rangle \langle n' | \frac{\partial H}{\partial k^\beta} | n \rangle - (\alpha \leftrightarrow \beta)}{(\epsilon_n - \epsilon'_n)^2} \tag{1.6}$$

where $|n\rangle$ and ϵ_n are the energy eigenstate and eigenvalue of Hamiltonian H, respectively. In the presence of an electric field ($\mathbf{E}$), the electron will acquire an anomalous velocity proportional to the Berry curvature [3]-

$$v_n(\mathbf{k}) = \frac{\delta \epsilon_n}{\hbar \delta \mathbf{k}} - \frac{e}{\hbar} \mathbf{E} \times \Omega_n(\mathbf{k}) \tag{1.7}$$

The first term is the group velocity of electrons driven by the electric field in momentum space. The second term is the anomalous velocity driven by the combined effect of the electric field and Berry curvature, which may contribute to AHE. If the crystal system has time-reversal symmetry, then the symmetry condition is [28]-

$$\Omega_n(-\mathbf{k}) = -\Omega_n(\mathbf{k})$$

If the crystal system has inversion symmetry, then the symmetry condition is [28]-

$$\Omega_n(-\mathbf{k}) = \Omega_n(\mathbf{k})$$

Hence, in a crystal where either time-reversal symmetry or inversion symmetry is broken, Berry curvature can give rise to AHE in the presence of strong SOC. The anomalous Hall conductivity

(AHC) arises due to the Berry curvature was evaluated by using the Kubo formula [30]-

$$\sigma_{\alpha\beta} = -\frac{e^2}{\hbar}\sum_n \int \frac{d^3k}{(2\pi)^3}\Omega^n_{\alpha\beta} f_n \tag{1.8}$$

where f_n is the Fermi distribution function, the momentum space Berry curvature is large wherever two electronic bands approach each other energetically and hybridize as a consequence of the combined effect of SOC and broken time-reversal symmetry [31, 32, 33]. The interband mixing under the influence of SOC may create band degeneracy or band splitting, and when the Fermi level resides within the SOC-induced band splitting, the Berry curvature experiences a sharp enhancement [31, 34, 35, 36]. The momentum space Berry curvature-induced σ_{xy} is purely linked with the electronic band structure. Therefore, it does not depend on τ ($\sigma_{xy} \propto \tau^0$), and thus, the intrinsic $\rho_{xy} = \frac{\sigma_{xy}}{\sigma^2_{xx}}$ will be proportional to the square of the ρ_{xx} ($\rho_{xy} \propto \rho^2_{xx}$) [3]. Because both the side jump and the momentum space Berry curvature induced ρ_{xy} show quadratic dependency on ρ_{xx}, it is not possible practically to separate out these contributions in AHE.

The intrinsic contribution of the AHE is calculated by integrating the Berry curvature over the whole Brillouin zone as shown in Eq. (1.8) [31, 34]. The existing symmetry element within the crystal structure plays a crucial role in deciding the net Berry curvature, and thus, AHE. Nonzero AHE is the result of the absence of symmetries like time-reversal symmetry and mirror operations that reverse the sign of local Berry curvature on reversing the sign of the momentum vector [31]. A strong AHE due to non-vanishing Berry curvature associated with the electronic band structure having non-trivial features like multiple band-contact points or nodal lines near the Fermi level, has been observed in various compounds such as $Co_3Sn_2S_2$ [37], and binary compounds like Mn_3Sn [38], Mn_3Ge [6], Fe_3Sn_2 [39, 40, 41, 42], Fe_5Sn_3 [43], Mn_3Pt [44], etc. A most recent study suggests that the electronic band splitting in the presence of SOC may also trigger large Berry curvature and, consequently, the AHE [35]. Therefore, the magnetic systems characterized by the band structure with non-trivial features, such as linear band crossings as a consequence of strongly hybridized electronic states, leading to the presence of band-touching points as well as band splitting near the Fermi level as a result of SOC, offer a promising platform for exploring the AHE.

Furthermore, a sign reversal in the intrinsic AHC of Mn_3Sn [45] and Mn_3Pt [44] compounds have

been reported under the variation in the orientation of spin polarization with temperature. Recently, extensive research has been carried out to understand the manipulation of sign and magnitude of AHE due to many factors, such as spin orientation [44, 45, 46, 47], the value of magnetization [48] and the interface induced SOC or breaking inversion symmetry [49]. In recent findings, a specific group of binary compounds like FeGe [50], MnGe [51, 52], MnAs [34], MnBi [53] has also been observed to exhibit the AHE. The AHE is valuable for spintronics, characterizing magnetization in small devices, and developing materials for data storage, magnetic sensors, and magnetoresistive random-access memory (MRAM) by enabling electron spin measurement and manipulation [3, 28, 54, 55, 56]. Although substantial progress has been made in understanding, the origin of AHE [1] has remained unclear for more than 5 decades. Extensive theoretical and experimental research has been carried out to develop a generalized perception and comprehensive understanding of AHE in different materials.

1.1.4 Topological Hall effect

In addition to the magnetic field-dependent OHE and magnetization-dependent AHE, a Hall contribution has been observed due to the real space non-coplanar magnetic spin textures. The additional Hall contribution is generally observed due to the mesoscopic topologically stable non-coplanar spin textures (size 100-200 nm) such as skyrmion, and therefore, named as topological Hall effect (THE) [57].

Topologically stable structure means exceptional stability of spin texture with non-trivial topology, and the corresponding topological number remains invariant under a continuous small external perturbation (like an external magnetic field or mechanical deformation) [59, 60]. Fig. 1.7 displays a comparison between topologically stable skyrmion and bubble (non-coplanar spin structure without topological stability), which indicates the skyrmion is stable upto a larger field as compared to the bubble, clearly demonstrates the meaning of topologically stable under the external perturbation of magnetic field [58]. The topological number or skyrmion number (S) is a measure of the winding of localized magnetization (**m**) about the unit sphere. The topological number can be expressed as [59, 60]-

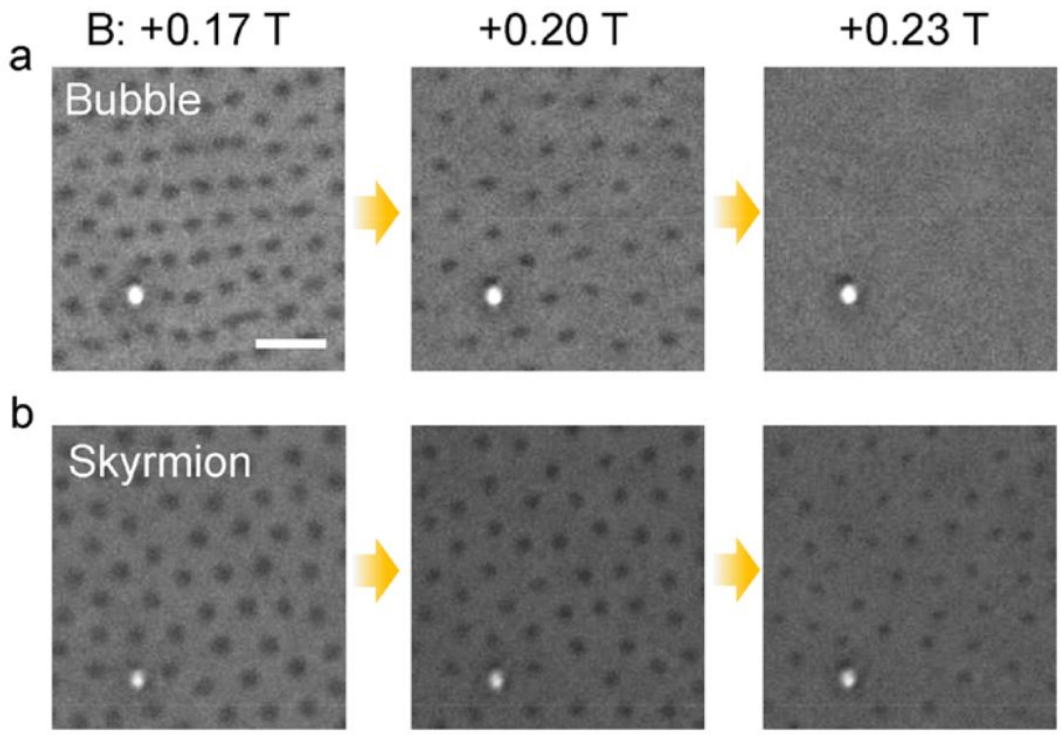

Figure 1.7: Magnetic field dependence of the bubble and the skyrmion phases. (a) Evolution of the bubble phase with increasing fields. (b) Evolution of the skyrmion phase with increasing fields [58].

$$S = \frac{1}{4\pi}\int \mathbf{m}(r).\left[\frac{\delta \mathbf{m}(r)}{\delta x} \times \frac{\delta \mathbf{m}(r)}{\delta y}\right] d^2r \tag{1.9}$$

In the presence of a non-coplanar magnetic texture with non-zero spin chirality or skyrmion, the charge carriers experience a fictitious magnetic field, which introduces a real space Berry phase in the eigenstate of the charge carriers, giving rise to THE [61, 62], as shown in Fig. 1.8. The THE is an effective tool for the electrical detection of these non-trivial phases [60]. Not only THE but there are also many other developed tools like neutron diffraction, Lorentz transmission electron microscopy (LTEM), magnetic force microscopy (MFM) [63] and spin-resolved scanning tunneling microscopy (STM), etc., for the direct detection of skyrmion [60].

Magnetic systems with large SOC and broken inversion symmetry are expected to have Dzyloshinskii-Moriya interaction (DMI), which is initially believed to be an essential mechanism for developing skyrmion-like non-coplanar spin structure [64]. The THE due to skyrmion-like topological spin textures has been detected in various non-centrosymmetric bulk chiral magnets, including B20

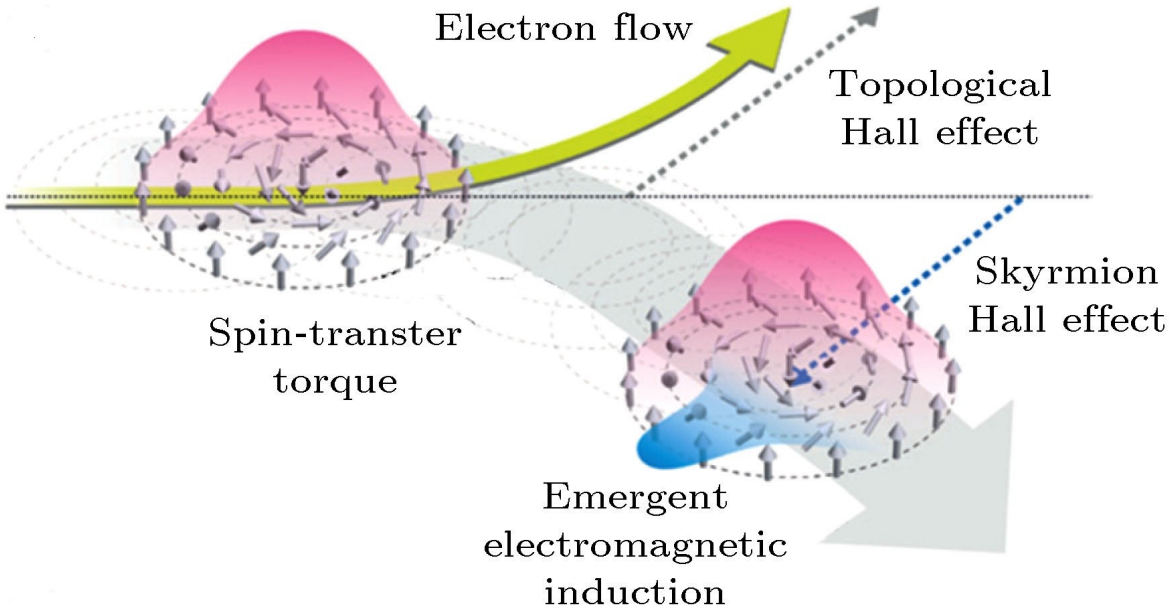

Figure 1.8: Schematic of electron motion as it traverses a skyrmion spin texture, generates the topological Hall effect, and the motion of skyrmions driven by an applied current, responsible for the skyrmionic Hall effect [60]

compounds [65, 66, 67], β-Mn type Co-Zn-Mn alloys [68], as well as in materials exhibiting non-centrosymmetric D_{2d} symmetry [69, 70, 71, 72, 73]. This non-trivial texture arises from the interplay between exchange interactions and chiral forces, such as bulk DMI. Instead of these bulk systems, multilayer heterostructures like $LaMnO_3/SrIrO_3$ [74], $SrRuO_3/SrIrO_3$ [75], $SrRuO_3/BaTiO_3$ [37], and $SrRuO_3/SrTiO_3$ [76], etc., are also found to exhibit a large THE due to such non-trivial magnetic textures that emerge as a result of the interfacial DMI.

Several theoretical studies suggest lattice imperfection-induced local DMI, which may be of a sizeable magnitude in defect-rich polycrystalline magnets [77, 78, 79]. This local DMI may give rise to the spin chiral non-coplanar spin texture/skyrmion, depending upon the strength and competition with other magnetic energy contributions [80, 81]. Recently, in Pd doped Mn_3Ga compound, the emergence of THE has been observed due to the spin chiral non-coplanar spin texture, developed because of the possible existence of DMI. The DMI is supported by local symmetry breaking caused by introducing substitutional defects within the crystal structure [82]. Nowadays, instead of the non-centrosymmetric compounds with DMI, the topological skyrmion-like spin texture has also been observed in centrosymmetric compounds like MnPdGa [83] and NiMnGa [84], as a result of the interplay between uniaxial magneto-crystalline anisotropy and magnetic dipole-dipole

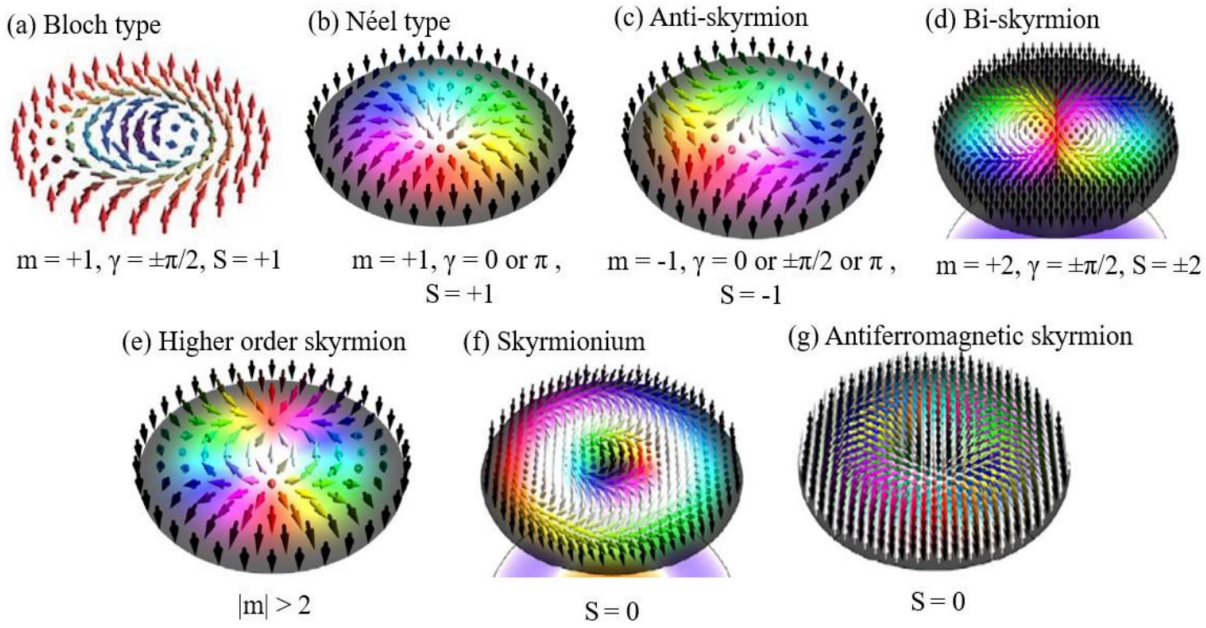

Figure 1.9: Various magnetic textures of skyrmion characterized by vorticity (m), helicity (γ), and topological number (S) [85].

interaction without the existence of DMI.

1.1.4.1 Types of skyrmion

There are two conventional types of magnetic skyrmions: Néel type (Fig. 1.9 (a)) and Bloch type (Fig. 1.9 (b)), characterized by vorticity (m), and helicity (γ) depending upon sense of rotation of magnetic moment from the center of the non-collinear magnetic texture to the periphery [85]. In a Bloch-type skyrmion, the spins rotate in the tangential planes, that is, perpendicular to the radial directions, when moving from the center to the periphery of the non-collinear magnetic texture [86]. Such spin texture is typically found in bulk systems of B-20 [65, 66, 67] and β-Mn type chiral compounds [68]. In a Néel-type skyrmion, the spins rotate in the radial planes from the core to the periphery of the non-collinear magnetic texture [86]. Néel skyrmions are generally realized in ultra-thin film heterostructures with broken inversion symmetry at the interface of two consequent thin layer [74, 75]. Therefore, the realization of these typical skyrmionic textures depends upon the underlying crystal symmetry or on the presence of an interface in a magnetic material. Their extremely small nanometer size, inherent high stability, dynamics and ultra-low current density requirement for manipulation make them potential candidates for the next generation energy-efficient information storage and logic technologies [60, 87, 88, 89, 90, 91].

The primary challenge hindering the practical use of skyrmions in daily life applications is the skyrmionic Hall effect (SHE) due to the transverse deflection of skyrmions when driven by the spin-polarized current [Fig. 1.8]. As a result of SHE, when the current is applied to the system, the skyrmions are pushed towards the edge of the system, leading to pinning or even loss of data [85]. This is one of the reasons why no skyrmion-based device exists today. There are many interesting theoretical predictions to suppress SHE, but they are challenging to realize. Since SHE depends on the topological number and rotational symmetry of non-trivial topological texture. Hence, the effective way to suppress SHE is to utilize nano-objects having the topological number (S) = 0 or objects with broken rotational symmetry. This means there is a need to explore more alternative topologically stable magnetic quasiparticles. Application-wise, Anti-skyrmion (Fig. 1.9 (c)) and bi-skyrmion [Fig. 1.9 (d)] are more attractive since they can move with negligible SHE because of the broken rotational symmetry [85]. The anti-skyrmion exhibits co-existence of Bloch and Néel type spin dynamics and typically emerges in the systems having non-centrosymmetric D_{2d} symmetry [70, 71, 86]. The bi-skyrmions are two closely spaced and interlocked skyrmions and generally observed in hexagonal centrosymmetric compounds [86]. In addition, there are many other theoretically predicted quasiparticles like higher-order skyrmion [Fig. 1.9 (e)] with broken rotational symmetry, and skyrmionium [Fig. 1.9 (f)] and antiferromagnetic skyrmion [Fig. 1.9 (g)] with zero topological number are potential candidates to suppress SHE and need experimental realization [85].

1.1.5 Possible origin of topological Hall effect

Besides skyrmions, the THE has also been observed due to the microscopic non-coplanar spin texture (size of a few nanometers) with non-vanishing spin chirality [$S_i.S_j \times S_k \neq 0$, where S_i, S_j, and S_k are three neighboring spins making a particular solid angle] [93] and therefore should be named the spin chirality Hall effect, according to a recent review article [63]. However, to be consistent with previous literature, we will proceed using THE. The different possible origin of THE is shown in Fig. 1.10. The non-coplanar spin structure with non-zero spin chirality and consequently large THE, has been realized in several frustrated magnets with triangular lattice such as Mn_5Si_3 [93], Mn_3Ga[94], Mn_3Sn [95], and $Fe_{1.3}Sb$ [96]. In these magnets, the evolution of such non-coplanar magnetic structure from the non-collinear magnetic structure occurs due to spin canting as a result

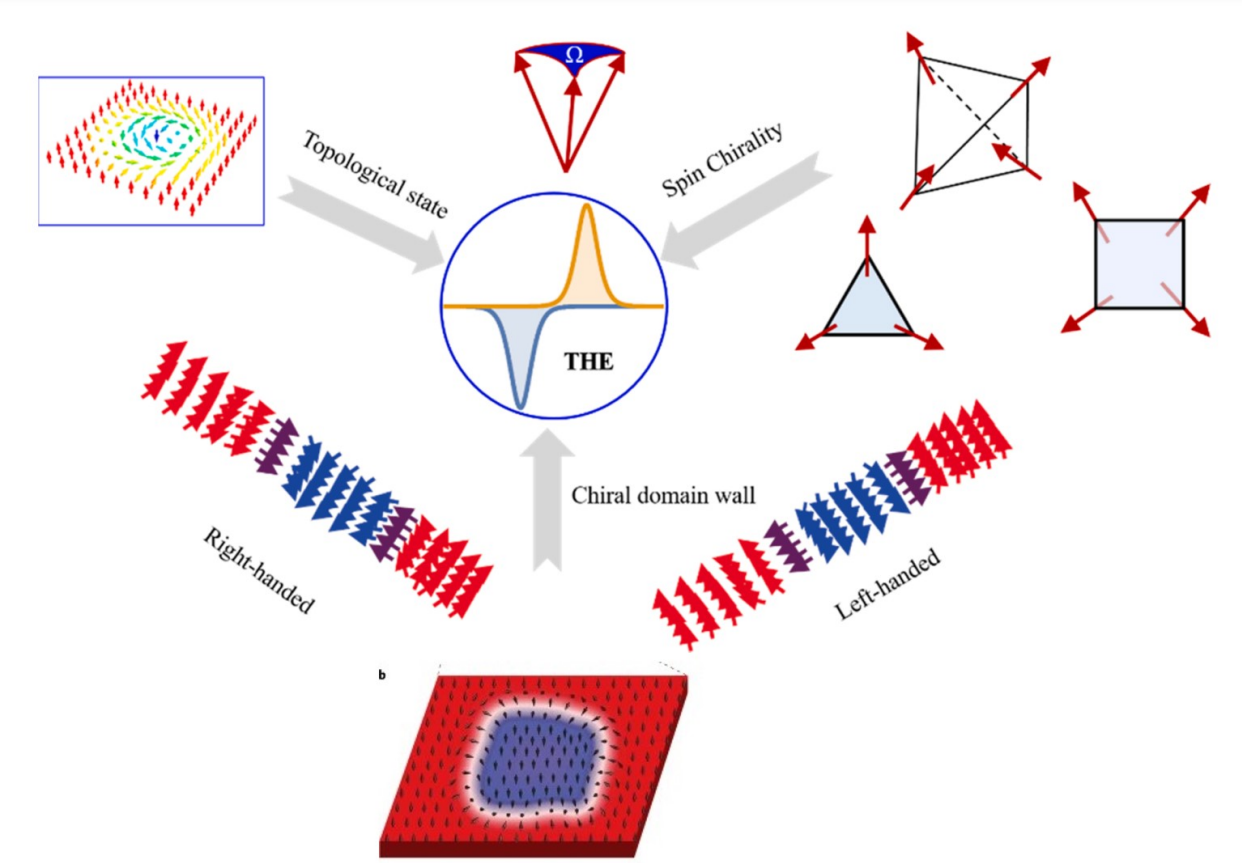

Figure 1.10: Topological Hall effect, caused by topological states like skyrmion, spin chirality on Kagome, triangular and pyrochlore lattice, and chiral (right- and left-handed) domain wall [92].

of the interplay between uniaxial magnetocrystalline anisotropy (MCA) and weak structural distortion/defect. In addition, Fe-doped Mn_3Sn [97, 98] and Mn_3Ge [99], and Kagome magnet YMn_6Sn_6 [100] with hexagonal crystal structure have recently been observed to exhibit a large THE due to the non-coplanar spin structure, which emerges as a result of the competition between Heisenberg exchange interactions and uniaxial MCA. The oxides with pyrochlore structure ($A_2M_2O_7$, where A = Nd, Pr, Y, Tb; M = Mo, Ir, V)), has also been found to exhibit THE due to the non-coplanar structure with scalar spin chirality associated with pyrochlore lattice within the unit cell [101]. The THE from chiral domain walls in the multi-domain state has been suggested in topological insulator heterostructures [102]. In addition to the interesting phenomena observed in transverse resistivity, such as the AHE and THE, the longitudinal resistivity (measured along the current direction) can also exhibit anomalous features like superconductivity [103], Kondo effect [104], and giant negative magnetoresistance [105]. In the present thesis, we have studied the Kondo effect in addition to the AHE and THE.

1.2 Kondo effect

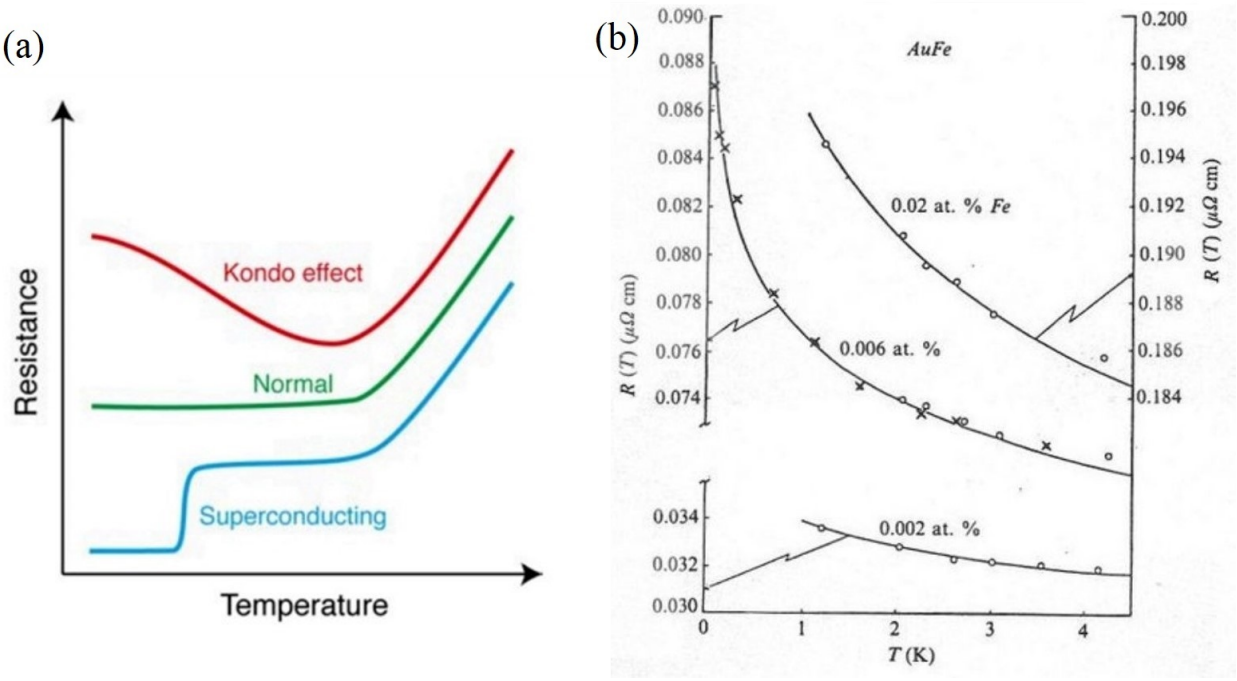

Figure 1.11: (a) Kondo effect in the metal (red line) as compared to normal metallic (green line) and superconducting (blue line) behavior [106]. (b) Variation in resistivity minima with the change in the percentage of Fe impurity [114].

In normal metal, resistivity decreases with a decrease in temperature because of lessened scattering of conduction electrons from lower lattice vibration called phonon. In very low-temperature regions, the resistivity drops gradually and is maintained up to absolute zero [green curve of Fig. 1.11 (a)] due to the scattering of electrons from phonon, defects such as dislocation and grain boundaries, or else impurities [107, 108, 109, 110]. On the other hand, some metals like lead, niobium, and aluminium demonstrate an anomalous drop in resistivity upto nearly zero below a critical temperature [blue curve of Fig. 1.11 (a)] and become superconducting [111]. Whereas in 1934, it was discovered that the electrical resistivity increases with the lowering of temperature in metallic systems [112], as shown by the red curve in Fig. 1.11 (a). After three decades, the origin has been explained due to magnetic impurities based on the studies reflecting the correlation between resistivity minima and the percentage of magnetic (Fe) impurity in metal (Au) [Fig. 1.11 (b)][113, 114, 115].

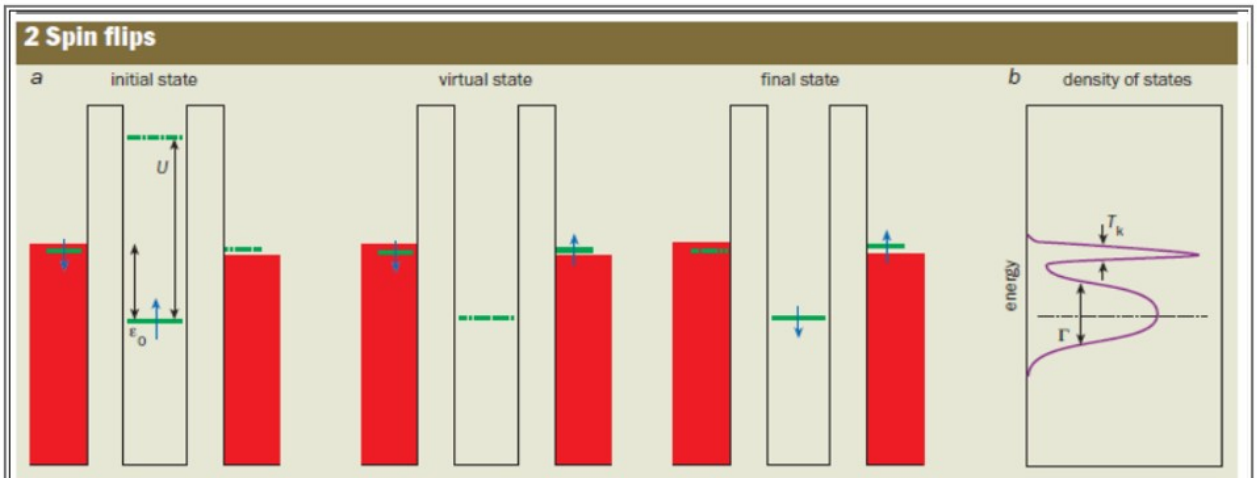

Figure 1.12: (a) Anderson model of magnetic impurity with one electron at energy level of ϵ_0 below the Fermi level of metal (red). The Fermi level is occupied by one spin down electron (blue). (b) Density of state as a function of energy [116].

1.2.1 Anderson model

In 1961, Anderson proposed the simplest model of magnetic impurity [115], which has only one electron at the energy level of ϵ_0 and width Γ [Fig. 1.12 (b)]. He has argued that the electron can quantum mechanically tunnel from the impurity and escape provided its energy lies above the Fermi level, otherwise, it remains trapped. Adding another electron is prohibited by the Coulomb energy, U, while it would cost at least energy of $|\epsilon_0|$ to remove the electron. Fig. 1.12 (a) depicts the transfer of an electron from a localized impurity state to an unoccupied energy state at the surface of Fermi sea, necessitating a substantial energy input, typically ranging from 1 to 10 eV for magnetic impurities (virtual state). While this process is classically forbidden, the Heisenberg uncertainty principle in quantum mechanics allows for the existence of such a configuration for a very brief period around $h/|\epsilon_0|$, where h is the Planck constant. Within this short time-frame, another electron must tunnel from the Fermi sea back to the impurity. Notably, the spin of this electron may be opposite to the initial spin of the impurity, resulting in the different initial and final spin states of the impurity. This phenomenon, known as the spin exchange process, triggers a spin excitation in the Fermi sea. When many such processes are considered collectively, they give rise to a distinct state referred to as the Kondo resonance at the Fermi level with the width of energy corresponding to Kondo temperature (T_k) [Fig. 1.12 (b)].

1.2.2 Kondo model

In 1964, Kondo explained how the internal spin flip of conduction electron and impurity during the scattering of conduction electrons from magnetic impurities affect resistivity [114]. Consider conduction electron with wave number k and spin-down ↓ collide with impurity in a state with spin up ↑ and scattered into a final state of wave number k′ with spin-down ↓, along with the impurity remains in a state with spin up ↑. The matrix element during this scattering process can be expressed as-

$$J(k\downarrow,\uparrow\rightarrow k'\downarrow,\uparrow) \tag{1.10}$$

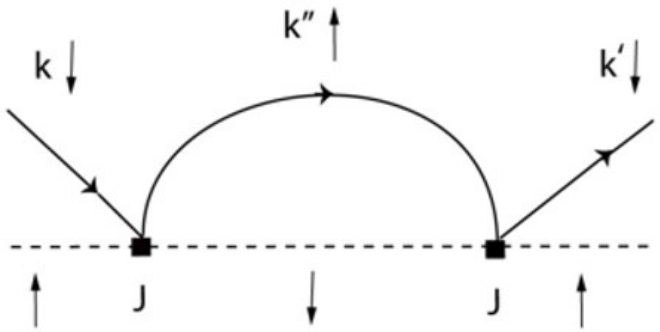

Figure 1.13: Schematic representation of the spin-flip scattering process in which a down-spin conduction electron (thick line) is scattered by the impurity (dotted line) into an intermediate spin-up state [117].

This type of scattering has initially been considered and J is the exchange coefficient. Kondo considered a higher-order correction term in Eq. (1.10) that involves intermediate state of spin-flip of impurity and conduction electron where the electron is scattered into the state with wave number k″ and spin up ↑ leaving the impurity is a spin down state ↓ after scattering before going to final state as in Eq. (1.10). The schematic representation of this scattering process is shown in Fig. 1.13. According to quantum mechanics, the total matrix element after a sum of k″ over all possible intermediate states involved in this scattering process is given by-

$$\sum_{k''} J(k\downarrow,\uparrow\rightarrow k''\uparrow,\downarrow).J(k''\uparrow,\downarrow\rightarrow k'\downarrow,\uparrow)\frac{1-f_{k''}}{\epsilon_k-\epsilon_{k''}} \tag{1.11}$$

where ϵ_k is the energy of electron with wave no. k and f_k is unity if the state k is occupied and 0 if it is empty. The term $1 - f_{k''}$ is taken to exclude an occupied state k$''$ from the sum. Let us assume J is a constant and the sum over k$''$ is replaced by the integral over the density of state $\rho_{k''}$, which is also assumed to be a constant. The Eq. (1.11) becomes-

$$J^2\rho \int \frac{1 - f_{k''}}{\epsilon_k - \epsilon_{k''}} dk'' = J^2\rho \int_{\epsilon_F}^{D} \frac{1}{\epsilon_k - \epsilon_{k''}} dk'' \tag{1.12}$$

In the above expression, we assume the electron energy takes a value between 0 and D, and the states below the Fermi level ϵ_F are occupied. For the occupied states below ϵ_F, f_k = 0. The result of the integral in Eq. (1.12) is-

$$J^2\rho log\left(\left|\frac{\epsilon_k - \epsilon_F}{\epsilon_k - D}\right|\right) \tag{1.13}$$

We must add the first term J to the above spin flip correction term to the matrix element-

$$J + J^2\rho log\left(\left|\frac{\epsilon_k - \epsilon_F}{\epsilon_k - D}\right|\right) \tag{1.14}$$

The scattering probability W_k of the electron is proportional to the square of the total matrix element, which gives-

$$W_k \propto J^2 + 2J^3\rho log\left(\left|\frac{\epsilon_k - \epsilon_F}{\epsilon_k - D}\right|\right) + O(J^4) \tag{1.15}$$

To calculate the resistivity, we must consider the electrons whose energy lies within a window of about k_BT about the Fermi energy. This means $|\epsilon_k - \epsilon_F| \approx k_B$T and find the resistivity of the form-

$$R(T) = R_0\left[1 + 2J\rho log\left(\left|\frac{k_BT}{D - \epsilon_F}\right|\right)\right] \tag{1.16}$$

Hence, the internal spin flip of the impurity and scattered electron could give rise to a resistivity contribution behaving as log(T) , and hence provide a satisfactory explanation of the observed

resistance minima. If J>0, then the interaction leads to align the spin of conduction electron and impurity in the same direction (ferromagnetic case). If J<0, then the interaction leads to align the spin of conduction electron and impurity in the opposite direction (antiferromagnetic case). Only in the antiferromagnetic case the extra scattering term give a contribution to the resistivity that increases as the temperature is lowered. The so-called Kondo temperature (T_k) is roughly a temperature at which the resistance starts to increase logarithmically. As the temperature is lowered (T tends to 0), the above expression diverges and the magnetic impurity spin screened out by conduction electron and behaves like non-magnetic impurity giving a temperature independent contribution to resistivity. In several systems, the very low temperature behaviour ($T << T_k$) of resistivity can be explained in term of a Fermi-liquid [118] or a non-Fermi liquid [119] of heavy quasi-particles (heavy fermion is electron with enhanced effective mass).

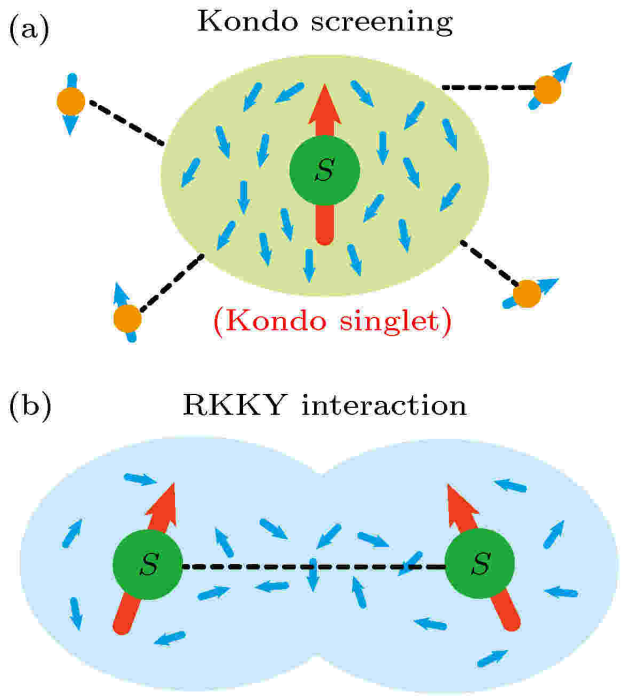

Figure 1.14: Sketch of the (a) Kondo screening, and (b) RKKY interaction [120].

The Kondo effect was subsequently explained in terms of antiferromagnetic exchange coupling between the delocalized conduction electrons and localized spins associated with the magnetic impurity atoms [115]. The localized spin is screened by conduction electron and gives rise to the Kondo effect, as shown in Fig. 1.14 (a). When the concentration of the magnetic impurity is sufficiently large, another resistivity minimum may appear above or below the Kondo minimum temperature

depending on whether the RKKY interaction between the spins [Fig. 1.14 (b)] is stronger or weaker than the Kondo coupling [118, 121, 122, 123, 124].

Kondo systems can show fascinating magnetic behavior as the localized spin S can interact with conduction electrons of the host matrix through n different orbital channels (name them like d_{xx}, d_{xy}, etc.) [125, 126] which in turn decides whether the spin will be (i) exactly compensated, leading to spin singlets giving rise to Fermi liquid behavior, (ii) under-compensated, leaving an effective spin degeneracy at low temperatures in zero field for magnetic elements with more than one spin configuration and (iii) over-compensated leading to quantum critical behavior as temperature and magnetic field tend to zero, giving rise to non-Fermi liquid behavior [125, 126, 127].

Since the initial discovery of the Kondo minimum in the temperature-dependent resistivity of dilute systems, this phenomenon has been observed in a wide array of materials, including graphene [128], indium tin oxide (ITO) nanowires [127], and quantum dots based on Ga-Al-As interfaces [129], all without the introduction of magnetic dopants. The presence of local magnetic spins in these systems primarily arises from defects and vacancies. For example, defects in graphene lead to an imbalance between its sublattices, resulting in the emergence of π-states with energies close to the Dirac point. When these states are singly occupied due to Coulomb repulsion, they give rise to a magnetic moment [130]. In the case of ITO nanowires, oxygen vacancies near Sn sites serve as magnetic impurities [127].

The Kondo effect has been the subject of extensive investigation within heavy fermion Ce, Yb, and U-based intermetallics and compounds. This phenomenon arises from the single-ion Kondo exchange interaction, where the localized 4f/5f moments hybridize with itinerant electrons, resulting in the creation of either dense Kondo lattices or Kondo insulators characterized by a finite band gap [131]. In these systems, the on-site Kondo interaction competes with long-range RKKY exchange interactions mediated by itinerant Landau quasiparticles, leading to the emergence of long-range ordered magnetic states [123, 132, 133, 134, 135, 136]. In certain compounds, non-thermal parameters such as pressure, magnetic fields, and composition have been manipulated to drive the system toward a quantum critical state, unveiling intriguing and exotic properties [135, 137, 138, 139]. In most heavy fermion systems, the long-range ordered anti-ferromagnetic or ferromagnetic phases

become evident at temperatures below the Kondo minimum temperature [140]. This thesis work is primarily focused on investigating and enhancing the understanding of the above mentioned intriguing transport properties (AHE, THE, and Kondo effect) in Mn-based intermetallic compounds.

1.3 Intermetallic compound

Intermetallic compounds are a class of metal alloys that form ordered solid compounds involving two or more metallic elements and optionally one or more non-metallic elements [141]. The intermetallic compounds are not only fascinating from the fundamental perspective owing to their rich functional properties but also for their potential applications, such as magnetic materials, superconductors, hydrogen storage, shape memory alloys, coating materials, and dental amalgams [142]. Particularly, Mn-based intermetallic compounds gained wide interest due to their exotic functional properties, such as large anomalous Hall [6] and Nernst effects [143], shape memory effect [144], magnetocaloric effect [145], skyrmionic phase [69], giant barocaloric [146] and baromagnetic effects [147], superconductivity [148] and many other properties, which make them useful candidates for potential applications in refrigeration, biomedical, aerospace, future spintronic devices, etc. [142]. In the present thesis work, we have studied the specific group of Mn-based intermetallic compounds such as Mn-based Heusler compound, Mn-based pnictide, Mn-based antiperovskite.

1.3.1 Mn-based Heusler compound

In 1903, Friedrich Heusler first discovered a ferromagnetic material Cu_2MnAl, although none of its constituent elements is magnetic at room temperature by itself [149, 150]. Heusler compounds are a large family of binary (X_3Z), ternary (X_2YZ and XYZ), and quaternary ($XX'YZ$) compounds, where X, X′, and Y are transition metals or lanthanides, and atom Z belongs to main group elements [151, 152, 153]. The Heusler compounds, a tunable class of materials, have recently gained tremendous interest in the field of spintronics [151, 152, 153, 154, 155]. The extensive tunability of the Heusler compounds, like modification in the crystal structure through chemical substitutions and structural motifs puts these systems particularly interesting from both fundamental physics and technological application point of view [152, 156, 157, 158, 159]. On the basis of stoichiometry and

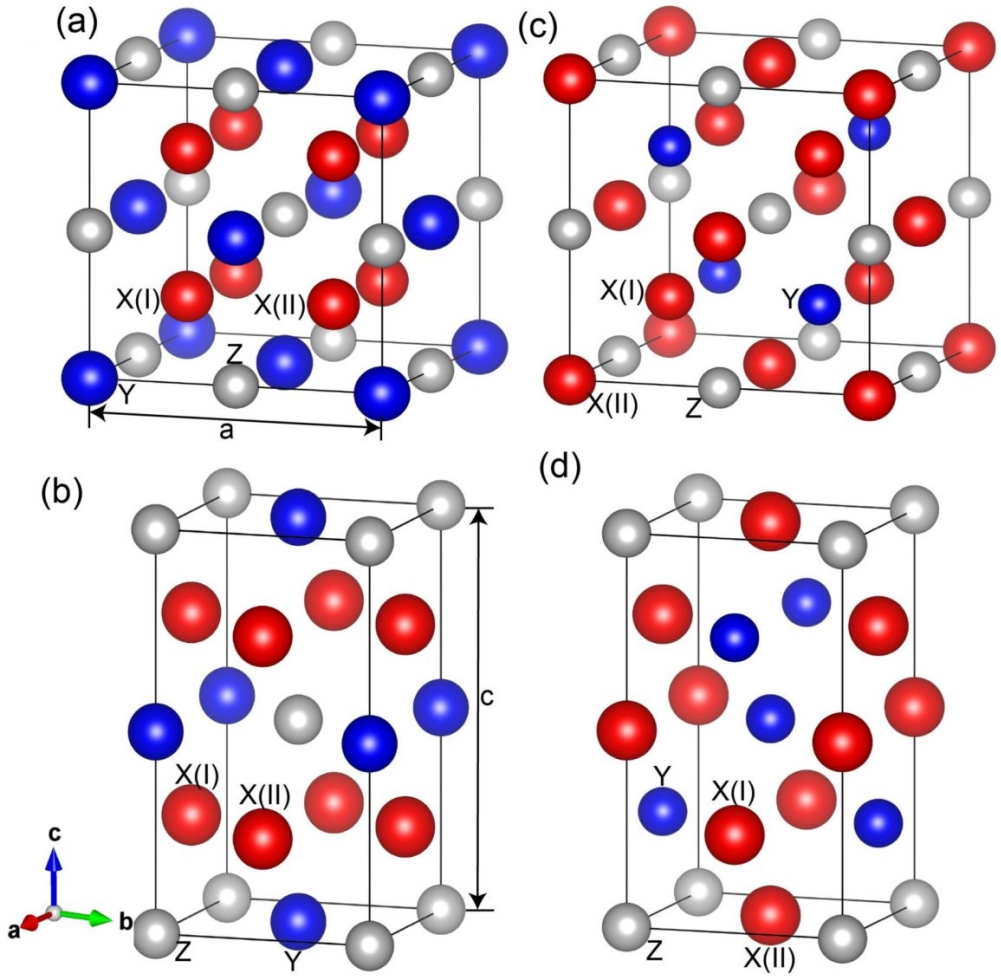

Figure 1.15: (a) Regular cubic Heusler structure. (b) Regular tetragonal Heusler structure. (c) Inverse cubic Heusler structure. (d) Inverse tetragonal Heusler structure [160].

crystal structure, Heusler compounds can be divided into three main classes: full-Heusler, inverse-Heusler, and half-Heusler [152].

Full Heusler compounds have complete Heusler composition X_2YZ (2:1:1) and can be divided into two groups of regular and inverse Heusler compounds [151]. Regular Heusler compounds exhibit either the face-centered cubic [centrosymmetric space group Fm-3m (225)] or the body-centered tetragonal [centrosymmetric space group I4/mmm (139)] crystal structure, as shown in Fig. 1.15 (a) and Fig. 1.15 (b), respectively [151]. Inverse Heusler compounds have an inverse crystal structure as compared to the regular Heuslers. Inverse Heuslers may crystallize in either face-centered cubic [non-centrosymmetric space group F-43m (216)]] or body-centered tetragonal [non-centrosymmetric space group I-4m2 (119)], as shown in Fig. 1.15 (c) and Fig. 1.15 (d), respectively [151]. Half-Heuslers are Heusler compounds with chemical composition of XYZ (1:1:1). The

half-Heusler compounds exhibit the same crystal structure as inverse Heuslers [151].

All the aforementioned Heusler classes are ternary. In addition to these, Heusler alloys are sometimes extended to binary and quaternary structures as a result of the structural variations and chemical substitutions. The Binary Heuslers with chemical composition X_2Z and X_3Z (for example Mn_2Sb, Fe_2Sb, Fe_3Al and Mn_3Ga,) exhibit the same crystal structure as the half and full Heusler compounds, respectively [151, 152]. Quaternary Heuslers have two different X atoms from transition group in the structure, forming chemical composition of XX′YZ, for example CoFeMnSi [151]. Quaternary Heuslers show the same crystal structure as half or inverse Heusler compounds [151].

Heusler compounds have recently attracted tremendous interest due to their exotic magneto-transport properties associated with the unique electronic band structure, which gives rise to non-trivial topological phases of matter, such as topological insulators, Dirac and Weyl semimetals [153]. Several Heusler systems such as Co_2MnGa [153], Co_2MnAl [161], and Co_2TiX (X=Si, Ge) [162] are found to exhibit large AHE originating from their unique band structure due to the combined effect of crystal structure and spin-orbit interaction. In recent years, the correlation between crystal structure and AHE has been widely studied in Co_2-based [156] and Fe_2- based Heusler compounds [163].

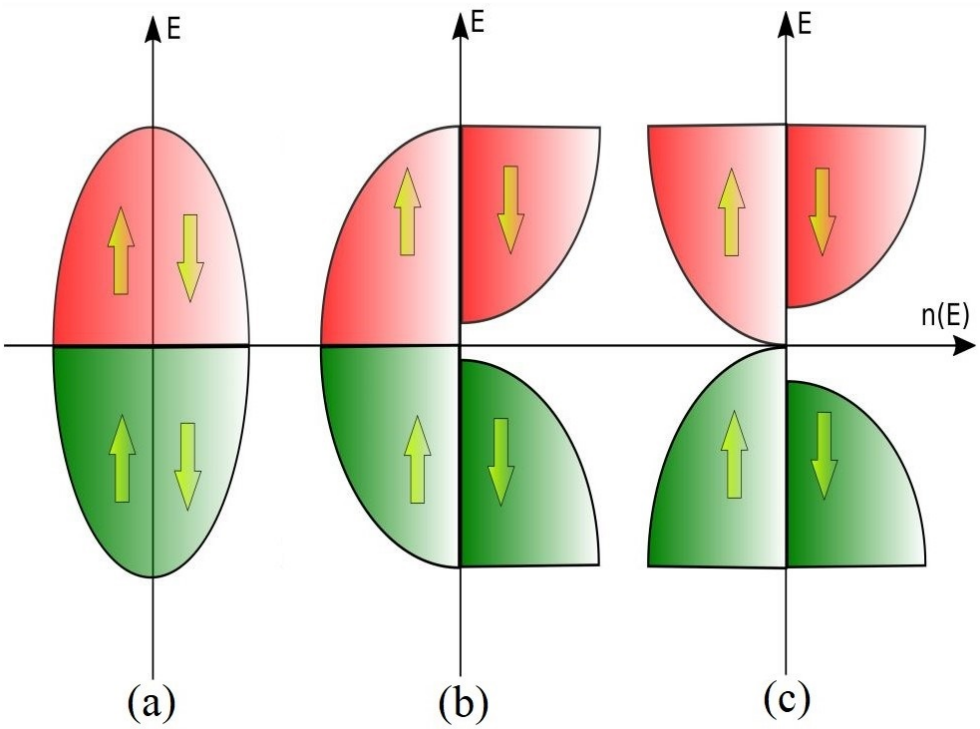

Figure 1.16: Density of state for (a) Metal (b) Half-metal (c) Spin-gapless semiconductor [181].

Among Heuslers, Mn-rich Heusler compounds have attracted a great deal of interest as spin gapless semiconducting and half-metallic ferri- and ferromagnets and as materials for spintronic applications [164]. Half-metals and spin-gapless semiconductors are a specific class of materials that have novel spin-dependent electronic properties, owing to their unique electronic structure [165]. The band structure of these materials have an energy gap for one spin state (minority spin down) in contrast to metal and the band gap disappears for the other spin state (minority spin up), as shown in Fig. 1.16. Fig. 1.16 (b) and (c) indicates that the only difference between the band structure of half metal and spin gapless semiconductor (SGS) is that the maxima of valence band and minima of conduction band for majority spin up channel touch each other at a point in the SGS, whereas in half metal these bands are completely overlapping on each other near the Fermi level [165]. This phenomenon leads to 100% spin-polarization and promising spin-controlled electronic and magnetic properties for spintronics applications [165, 166]. Another important difference between a half-metal and SGS is the value of AHC at room temperature, SGSs generally have about one order less AHC as compared to the half-metals [165].

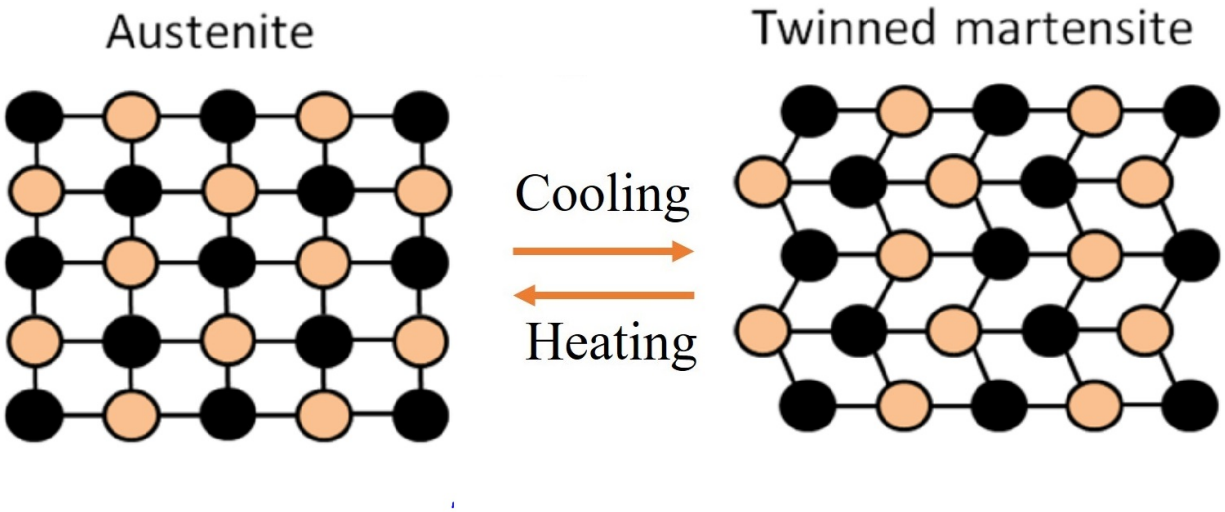

Figure 1.17: Schematic diagram of thermally driven martensitic transition [180].

In addition to the aforementioned properties, Mn-rich Heuslers show other fascinating multi-functional properties like magneto-caloric effect [167], shape memory effect [144], THE [69, 70, 71, 72, 73], etc. Mn-based Heusler compound with shape memory effect exhibit thermally activated structural phase transition from high temperature austenite (cubic) to low temperature martensite (tetragonal) phase [168, 169, 170, 171] [Fig. 1.18], may provide a perfect platform to better understand the cor-

relation between crystal symmetry and electronic transport properties of materials. A similar study has recently been done on Ni_2MnGa magnetic shape memory (MSM) Heusler compound experimentally, in which a large intrinsic anomalous Hall conductivity (IAHC) ∼57.9 S/cm has been observed in low-temperature tetragonal phase as compared to the IAHC of ∼21.5 S/cm in the high-temperature cubic phase [172]. This study indicates the intrinsic mechanism is getting suppressed when moving toward the highly symmetric cubic crystal system.

Particularly, Mn-based inverse Heusler compounds are interesting for realization of skyrmion like topologically stable spin texture because of their low saturation magnetization, low damping and high Curie temperature [173]. Notably, these compounds often exhibit competition between ferromagnetic and antiferromagnetic exchange interactions, which may lead to non-collinear magnetic texture [174, 175, 176]. In spintronics, one of the critical challenges is to find suitable materials that can retain their magnetic properties at room temperature or higher temperature [177]. In this context, the high Curie temperature Mn-based inverse Heusler compounds, which exhibits low saturation magnetization and low damping, is a potential candidate to explore skyrmion like non-trivial spin texture [178, 179].

1.3.2 Mn-based pnictide

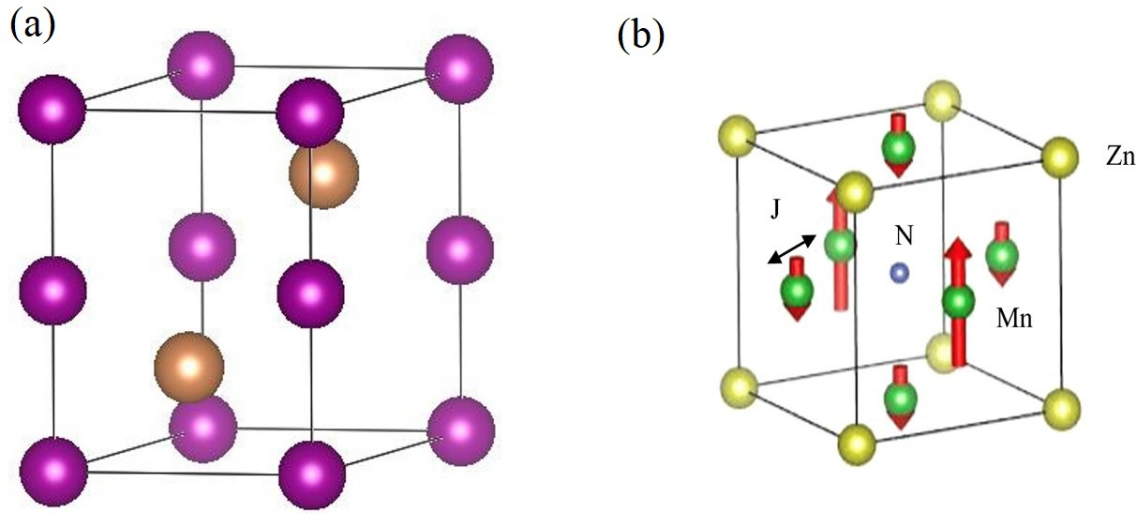

Figure 1.18: Crystal structure of (a) Mn-based binary pnictide; (b) Mn-based antiperovskite [182].

A pnictogen is the group (V) elements of the periodic table, which is also known as nitrogen group

or nitrogen family. Group (V) consists of the elements nitrogen (N), phosphorus (P), arsenic (As), antimony (Sb), bismuth (Bi), and moscovium (Mc) [183]. Binary compounds having a single element from the group (V) can be referred to collectively as pnictides. A theoretical study on Mn-based pnictides with formula MnX (X=N, P, As, Sb) suggests the occurrence of exciting properties like unique electronic band structure, elastic properties and mechanisms of superconductivity under high pressure [184]. The Mn-pnictides like MnBi, MnSb, MnAs with NiAs-type hexagonal structures [Fig. 1.18 (a)] gained renewed recognition in high-temperature spintronics research due to their high Curie temperature, spin reorientation transition (SRT), and large uniaxial magneto-crystalline anisotropy with the magnetic easy axis parallel to the c-axis of the crystal system [185, 186, 187, 188, 189, 190]. These fascinating properties of Mn-pnictides make it a potential candidate for comprehensive magneto-transport studies such as AHE and THE.

1.3.3 Mn-based antipervoskite

Antiperovskites (or inverse perovskite), which are derived from perovskites, are the most adaptable and well-studied crystal structure [191]. Antiperovskites have stoichiometry X_3BA with cubic structure and Pm-3m space group [Fig. 1.18 (b)], same as perovskites with a general formula ABX_3 [191]. The key difference is that the positions of the cation and anion constituents are reversed in the unit cell structure as compared to the perovskites. Antiperovskites constitute an important class of materials with potential for a diverse range of technologically important functional and multifunctional properties like geometrically frustrated magnetism [192, 193, 194, 195], giant magnetoresistivity [196], magnetostriction [197, 198], magnetocaloricity [199, 200], superionic conductivity [201, 202, 203], superconductivity [204, 205], meta-thermal expansivity [206, 207, 208, 209], electrocatalysis [210], luminescence [211, 212], to name a few. The structure of these antiperovskites offers enormous flexibility in accommodating various chemical substitutions at the three sites and, thereby scope for improving the functional behavior of these materials. Among these antiperovskite compounds, the Mn-based antiperovskites with the chemical formula Mn_3BA, where B can be Ni, Ga, Sn, Cu, etc. while A can be C, N, B, have attracted a lot of attention in recent years due to their large negative thermal expansion [213, 214, 215, 216], large magnetovolume effect [217], giant barocaloric effect [146], large AHE [218, 219, 220, 221], anomalous Nernst effect [143, 222]

and electrical switching of spin-orbit torque [223].

1.4 Objective of the present work

The Mn-based intermetallic compounds, which facilitate high Curie temperature [178, 179, 185, 186, 187, 188, 189, 190] and the enormous flexibility of accommodating various kind of structural defects [224, 225, 226, 227, 228] and magnetic transitions [185, 186, 187, 188, 189, 190], are not only potential platform to establish a correlation between crystal structure, magnetic structure, Berry curvature, and magneto-transport properties but also for real-life applications of spintronic-based devices. Notably, these compounds typically exhibit significant magnetocrystalline anisotropy [229, 230] that may give rise to the THE due to the emergence of the microscopic non-coplanar spin textures or mesoscopic skyrmions, which is promising for future energy-efficient data storage-based spintronic devices [60, 87, 88, 89, 90, 91]. Furthermore, magnetic impurities arising due to defects/disorders may give rise to other exotic transport phenomena, such as the Kondo effect [104].

The discovery of the spin gapless semiconducting behavior in a Mn-rich Heusler compound, Mn_2CoAl, puts this material forward as an important candidate for technological application in the field of spintronics [11, 14, 179, 231]. Experimental studies on thin film as well as bulk systems of Mn_2CoAl reflect that most of the systems crystallize with compositional and/or anti-site disorder [227, 228, 232, 233, 234, 235, 236, 237, 238, 239, 240]. Theory suggests that the AHC, due to Berry curvature in the Mn_2CoAl compound, should be close to zero as a consequence of the broken time-reversal and space-inversion symmetry. However, the reported experimental value of AHC is not consistent with the theory [231]. A theoretical investigation considering anti-site disorder suggests an enhancement in AHC, necessitating a detailed experimental and theoretical investigation to understand the origin of AHC in the Mn_2CoAl Heusler compound [241]. Our objective is to investigate the crystal structure and AHE in the Mn_2CoAl compound through both experimental and theoretical approaches.

Recently, skyrmionic THE has been observed in the thin film form of the Mn_2CoAl compound due to interfacial DMI in the system [242]. Although the Mn_2CoAl compound is non-centrosymmetric (space group $F\bar{4}3m$), but the space group do not support bulk DMI (similar to the centrosymmetric magnets) as per the reported analysis on the point group dependency of micromagnetic DMI [243].

Interestingly, the literature suggests a strong magnetic frustration due to the presence of both ferro- and antiferromagnetic type Heisenberg exchange interaction along with the disorder in the Mn_2CoAl compound [175, 176, 240]. Therefore, the competition between the cubic MCA, which is expected in the cubic crystal systems [229], and the Heisenberg exchange interactions may create the non-coplanar spin texture [97, 100, 148, 229]. Our aim is to search for the THE resulting from the anticipated non-coplanar magnetic texture in the bulk Mn_2CoAl compound.

Another class of Mn-based Heusler compounds that exhibit the AHE and shape memory effect featuring the structural phase transition from high-temperature austenite (cubic) phase to low-temperature martensite (tetragonal) phase [168, 169, 170, 171], are fruitful candidates to establish whether there is any straightforward connection between crystal structure, Berry curvature and anomalous transport phenomena. Our aim is to study the different aspects of the scattering mechanism in the Mn_2NiGa MSM Heusler compound by analyzing the resistivity, magnetoresistance, and Hall data.

A recent study on a Mn-pnictide, MnAs compound has been demonstrated the SOC-induced band splitting and enhanced intrinsic AHC depending on the magnetization orientation [34, 36]. This observation inspired us to explore other Mn pnictides. The electronic band structure and magnetic state of the MnSb Mn-pnictide suggest significant hybridization between the Mn 3d and Sb 5p orbitals, which is responsible for the stabilization of the ferromagnetic state as compared to the other 3d transition metal mono-antimonides [185]. A neutron diffraction study [244] and a recent magneto-transport study [188] in a composition close to MnSb indicates the presence of spin reorientation transition (SRT) and AHE, respectively. Our objective is to investigate the AHE in a pure stoichiometric MnSb compound using both experimental and theoretical methods to explore the effect of SRT on the strongly hybridize electronic band structure and the AHE.

Very recently, in a similar Mn pnictide, MnBi, the THE has been discovered due to the microscopic non-coplanar spin structure and the mesoscopic topological skyrmionic bubble, resulting from the uniaxial magnetocrystalline anisotropy [230]. This finding motivated us to search for the possible THE in the MnSb compound with large uniaxial magneto-crystalline anisotropy. Therefore, we also aim to search the THE due to the possible emergence of skyrmionic bubble and/or microscopic non-coplanar magnetic structure in the MnSb compound.

Besides the Mn-rich Heusler compounds and Mn-based pnictides, the Mn-based antiperovskite nitrides offer exotic transport properties such as AHE [224] and anomalous Nernst effect [143, 222] due to their ability to accommodate atomic disorder/displacement at any of the three atomic sites [224, 225, 226]. Our objective is to analyze the temperature-dependent resistivity data in order to search the Kondo effect due to a very small fraction of Mn spins occupying the Ga lattice sites in a geometrically frustrated antiferromagnetic compound Mn_3GaN, belonging to the family of Mn-based antiperovskite nitrides.

In a similar Mn-based antiperovskite nitride, Mn_3SnN, the AHE has been observed due to the weak magnetic moment induced by spin canting from Γ^{5g} antiferromagnetic spin configuration [224]. The spin canting occurs due to structural symmetry lowering induced by large displacements of the magnetic manganese atoms away from high-symmetry positions. Similar atomic displacement has also been expected in the Mn_3GaN compound [224]. Our aim is also to investigate the AHE in the Mn_3GaN compound due to the possible spin canting from Γ^{5g} antiferromagnetic spin configuration.

References

[1] E. H. Hall, On a New Action of the Magnet on Electric Currents. Am. J. Math. **2**, 287 (1879).

[2] XVIII. On the "Rotational Coefficient" in nickel and cobalt. E. Hall, Philos. Mag. **12**, 157 (1881).

[3] N. Nagaosa, J. Sinova, S. Onoda, A. H. MacDonald, and N. P. Ong, Anomalous Hall effect. Rev. Mod. Phys. **82**, 1539 (2010).

[4] Y. Tian, L. Ye, and X. Jin, Proper Scaling of the Anomalous Hall Effect. Phys. Rev. Lett. **103**, 087206 (2009).

[5] R. Yu, W. Zhang, H.-J. Zhang, S.-C. Zhang, X. Dai, and Zhong Fang, Quantized Anomalous Hall Effect in Magnetic Topological Insulators. Science **329**, 61-64 (2010).

[6] A. K. Nayak, J. E. Fischer, Y. Sun, B. Yan, J. Karel, A. C. Komarek, C. Shekhar, N. Kumar, W. Schnelle, J. Kübler, C. Felser, and S. S. P. Parkin, Large anomalous Hall effect driven by a nonvanishing Berry curvature in the noncolinear antiferromagnet Mn_3Ge. Sci. Adv. **2**, e1501870 (2016).

[7] C.-Z. Chang, J. Zhang, X. Feng, Jie Shen, Z. Zhang, M. Guo, K. Li, Y. Ou, P. Wei, L.-L. Wang, Z.-Q. Ji, Y. Feng, S. Ji, X. Chen, J. Jia, X. Dai, Z. Fang, S.-C. Zhang, K. He, Y. Wang, L. Lu, X.-C. Ma, and Q.-K. Xue, Experimental Observation of the Quantum Anomalous Hall Effect in a Magnetic Topological Insulator. Science **340**, 167-170 (2013).

[8] T. Taniguchi, J. Grollier, and M. D. Stiles, Spin-Transfer Torques Generated by the Anomalous Hall Effect and Anisotropic Magnetoresistance. Phys. Rev. Appl. **3**, 044001 (2015).

[9] S.-Y. Yang, Y. Wang, B. R. Ortiz, D. Liu, J. Gayles, E. Derunova, R. G.-Hernandez, L. $\check{S}$mejkal, Y. Chen, S. S. P. Parkin, S. D. Wilson, E. S. Toberer, T. McQueen, and M. N. Ali, Giant, unconventional anomalous Hall effect in the metallic frustrated magnet candidate, KV_3Sb_5. Sci. Adv. **6**, eabb6003 (2020).

[10] G. E. Bauer, E. Saitoh , and B. J. v. Wees, Spin caloritronics. Nat. Mater. **11(5)**, 391-9 (2012).

[11] S. K. Kim, G. S. D. Beach, K. J. Lee, T. Ono, T. Rasing, and H. Yang, Ferrimagnetic spintronics. Nat. Mater. **21**, 24–34 (2022).

[12] T. Jungwirth, X. Marti, P. Wadley, and J. Wunderlich, Antiferromagnetic spintronics. Nat. Nanotechnol. **11**, 231–241 (2016).

[13] L. Šmejkal, Y. Mokrousov, B. Yan, and A. H. MacDonald, Topological antiferromagnetic spintronics. Nat. Phys. **14**, 242–251 (2018).

[14] S.D. Bader, S.S.P. Parkin, Spintronics. Annu. Rev. Condens. Matter. Phys. **1**, 71–88 (2010).

[15] A. Gerber, Towards Hall effect spintronics. J. Magn. Magn. Mater. **310**, 2749-2751 (2007).

[16] J. Moritz, B. Rodmacq, S. Auffret, and B. Dieny, Extraordinary Hall effect in thin magnetic films and its potential for sensors, memories and magnetic logic applications. J. Phys. D: Appl. Phys. **41**, 135001 (2008).

[17] R. Karplus, and J. M. Luttinger, Hall Effect in Ferromagnetics. Phys. Rev. **95**, 1154 (1954).

[18] M. C. Chang, Q. Niu, Berry phase, hyperorbits, and the Hofstadter spectrum: Semiclassical dynamics in magnetic Bloch bands. Phys. Rev. B **53**, 7010 (1996).

[19] A. Bohm, A. Mostafazadeh, H. Koizumi, Q. Niu, and J. Zwanziger, The Geometric Phase in Quantum Systems. Springer, Berlin (2003).

[20] J. Smit, The spontaneous hall effect in ferromagnetics I., Physica Amsterdam **21**, 877 (1955).

[21] S.-Y. Yang, Y. Wang, B. R. Ortiz, D. Liu, J. Gayles, E. Derunova, R. G.-Hernandez, L. mejkal, Y. Chen, S. S. P. Parkin, S. D. Wilson, E. S. Toberer, T. McQueen, M. N. Ali, Giant, unconventional anomalous Hall effect in the metallic frustrated magnet candidate, KV_3Sb_5. Sci. Adv. **6** eabb6003 (2020).

[22] G. Zheng, C. Tan, Z. Chen, M. Wang, X. Zhu, S. Albarakati, M. Algarni, J. Partridge, L. Farrar, J. Zhou, W. Ning, M. Tian, M. S. Fuhrer, and L. Wang, Electrically controlled superconductor-to failed insulator transition and giant anomalous Hall effect in kagome metal CsV_3Sb_5 nanoflakes. Nat. Commun. **14** 678 (2023).

[23] L. Berger, Influence of spin-orbit interaction on the transport processes in ferromagnetic nickel alloys, in the presence of a degeneracy of the 3d band. Phys. Rev. B **2**, 4559 (1970).

[24] C. L. Chien, C. R. Westgate, The Hall Effect and Its Applications, (1980).

[25] R. E. Prange, and S. M. Girvin, Eds., The Quantum Hall Effect (Springer, Berlin) (1987).

[26] D. J. Thouless, M. Kohmoto, M. P. Nightingale, and M. den Nijs, Phys. Rev. Lett. **49**, 405 (1982).

[27] Y. F.Zhao, R. Zhang, R. Mei, L.-J. Zhou, H. Yi, Y.-Q. Zhang, J. Yu, R. Xiao, K. Wang, N. Samarth, M. H. W. Chan, C.-X. Liu, and C.-Z. Chang, Tuning the Chern number in quantum anomalous Hall insulators. Nature **588**, 419–423 (2020).

[28] D. Xiao, M.-C. Chang, Q. Niu, Berry phase effects on electronic properties. Rev. Mod. Phys., **82**, 1959-2007 (2010).

[29] N. P. Ong, W. L. Lee, Geometry and the anomalous hall effect in ferromagnets. In Proceedings of the 8th International Symposium on Foundations of Quantum Mechanics in the Light of New Technology, ISQM-Tokyo 2005 (pp. 121-126) (2006).

[30] M. Gradhand, D. V. Fedorov, F. Pientka, P. Zahn, I. Mertig, and B. L. Györffy, First-principle

calculations of the Berry curvature of Bloch states for charge and spin transport of electrons, J. Phys.: Condens. Matter. **24**, 213202 (2012).

[31] Y. Yao, L. Kleinman, A. H. MacDonald, J. Sinova, and T. Jungwirth, D.-s. Wang, E. Wang, and Q. Niu. First-principles calculation of anomalous Hall conductivity in ferromagnetic bcc Fe. Phys. Rev. Lett. **92**, 037204 (2004).

[32] O. Stejskal, M. Veis, and J. Hamrle, The flow of the Berry curvature vector field. Sci. Rep. **12**, 97 (2022).

[33] N. Lazić and V Damljanović and M Damnjanović. Fully linear band crossings at high symmetry points in layers: classification and role of spin-orbit coupling and time reversal. J. Phys. A Math. Theor. **55**, 325202 (2022).

[34] C. Helman, A. Camjayi, E. Islam, M. Akabori, L. Thevenard, C. Gourdon, and M. Tortarolo, Anomalous Hall effect in MnAs: Intrinsic contribution due to Berry curvature, Phys. Rev. B **103**, 134408 (2021).

[35] G. K. Shukla, J. Sau, V. Kumar, M. Kumar, and S. Singh, Band splitting induced Berry flux and intrinsic anomalous Hall conductivity in the NiCoMnGa quaternary Heusler compound. Phys. Rev. B **106**, 045131 (2022).

[36] J. L. Ma, H. L. Wang, X. L. Wang, and J. H. Zhao, Experimental evidence for an anisotropic Berry-phase effect on the anomalous Hall effect in MnAs films, Phys. Rev. B **97**, 064402 (2018).

[37] L. Wang, Q. Feng, Y. Kim, R. Kim, K. H. Lee, S. D. Pollard, Y. J. Shin, H. Zhou, W. Peng, D. Lee, W. Meng, H. Yang, J. H. Han, M. Kim, Q. Lu, and T. W. Noh, Ferroelectrically tunable magnetic skyrmions in ultrathin oxide heterostructures. Nat Mater **17** 1087–1094 (2018).

[38] S. Nakatsuji, N. Kiyohara, and T. Higo, Large anomalous Hall efect in a non-collinear antiferromagnet at room temperature. Nature **527**, 212–215 (2015).

[39] L. Ye, M. Kang, J. Liu, F. von Cube, C. R. Wicker, T. Suzuki, C. Jozwiak, A. Bostwick, E. Rotenberg, D. C. Bell, L. Fu, R. Comin, and J. G. Checkelsky, Massive Dirac fermions in a ferromagnetic kagome metal. Nature **555**, 638–642 (2018).

[40] J. X. Yin, S. S. Zhang, H. Li, K. Jiang, G. Chang, B. Zhang, B. Lian, C. Xiang, I. Belopolski, H. Zheng, T. A. Cochran, S. Y. Xu, G. Bian, K. Liu, T. R. Chang, H. Lin, Z. Y. Lu, Z. Wang, S. Jia, W. Wang, and M. Z. Hasan, Giant and anisotropic many-body spin–orbit tunability in a strongly correlated kagome magnet. Nature **562**, 91–95 (2018).

[41] Q. Wang, S. Sun, X. Zhang, F. Pang, and H. Lei, Anomalous Hall effect in a ferromagnetic Fe_3Sn_2 single crystal with a geometrically frustrated Fe bilayer kagome lattice. Phy. Rev. B **94**, 075135 (2016).

[42] T. Kida, L. A. Fenner, A. A. Dee, I. Terasaki, M. Hagiwara, and A. S. Wills, The giant anomalous Hall effect in the ferromagnet Fe_3Sn_2 - a frustrated kagome metal. J. Phys.: Condens. Matter. **23** 112205 (2011).

[43] H. Li, B. Zhang, J. Liang, B. Ding, J. Chen, J. Shen, Z. Li, E. Liu, X. Xi, G. Wu, Y. Yao, H. Yang, and W. Wang, Large anomalous Hall effect in a hexagonal ferromagnetic Fe_5Sn_3 single crystal. Phys. Rev. B **101**, 140409 (2020).

[44] J. Mukherjee, T. S. Suraj, H. Basumatary, K. Sethupathi, and K. V. Raman, Sign reversal of anomalous Hall conductivity and magnetoresistance in cubic noncollinear antiferromagnet Mn_3Pt thin films. Phys. Rev. Materials **5**, 014201 (2021).

[45] P. K. Muduli, T. Higo, T. Nishikawa, D. Qu, H. Isshiki, K. Kondou, D. Nishio-Hamane, S. Nakatsuji, and YoshiChika Otani, Evaluation of spin diffusion length and spin Hall angle of the antiferromagnetic Weyl semimetal Mn_3Sn. Phys. Rev. B **99**, 184425 (2019).

[46] R. Ibarra, E. Lesne, B. Sabir, J. Gayles, C. Felser, A. Markou, Anomalous Hall Effect in Epitaxial Thin Films of the Hexagonal Heusler MnPtGa Noncollinear Hard Magnet. Adv. Mater. Interfaces **9**, 2201562 (2022).

[47] M. S. Alam, A. Fakhredine, M. Ahmad, P. K. Tanwar, H.-Y. Yang, F. Tafti, G. Cuono, R. Islam, B. Singh, A. Lynnyk, C. Autieri, and M. Matusiak, Sign change of anomalous Hall effect and anomalous Nernst effect in the Weyl semimetal CeAlSi. Phys. Rev. B **107**, 085102 (2023).

[48] D. J. Groenendijk, C. Autieri, T. C. Van Thiel, W. Brzezicki, J. R. Hortensius, D. Afanasiev, N. Gauquelin, P. Barone, K. H. W. Van Den Bos, S. Van Aert, J. Verbeeck, A. Filippetti, S. Picozzi,

M. Cuoco, and A. D. Caviglia, Berry phase engineering at oxide interfaces, Phys. Rev. Res. **2**, 023404 (2020).

[49] T. C. Van Thiel, W. Brzezicki, C. Autieri, J. R. Hortensius, D. Afanasiev, N. Gauquelin, D. Jannis, N. Janssen, D. J. Groenendijk, J. Fatermans, S. Van Aert, J. Verbeeck, M. Cuoco, and A. D. Caviglia, Coupling Charge and Topological Reconstructions at Polar Oxide Interfaces, Phys. Rev. Lett. **127**, 127202 (2021).

[50] C. S. Spencer, J. Gayles, N. A. Porter, S. Sugimoto, Z. Aslam, C. J. Kinane, T. R. Charlton, F. Freimuth, S. Chadov, S. Langridge, J. Sinova, C. Felser, S. Blügel, Y. Mokrousov, and C. H. Marrows, Helical magnetic structure and the anomalous and topological Hall effects in epitaxial B20 $Fe_{1-y}Co_yGe$ films. Phys. Rev. B **97**, 214406 (2018).

[51] Y. Fujishiro, N. Kanazawa, R. Kurihara, H. Ishizuka, T. Hori, F. S. Yasin, X. Yu, A. Tsukazaki, M. Ichikawa, M. Kawasaki, N. Nagaosa, M. Tokunaga, and Y. Tokura, Giant anomalous Hall effect from spin-chirality scattering in a chiral magnet. Nat. Commun. **12**, 317 (2021).

[52] H. Ishizuka, and N. Nagaosa, Spin chirality induced skew scattering and anomalous Hall effect in chiral magnets. Sci. Adv. **4**, eaap9962 (2018).

[53] M. Tang, Q. L. Wang, S. M. Zhou, W. J. Fan, X. P. Qiu, Anomalous Hall effect of MnBi films with perpendicular magnetic anisotropy. J. Alloys Compd. **820**, 153080 (2020).

[54] H. Ohno, D. Chiba, F. Matsukura, T. Omiya, E. Abe, T. Dietl, Y. Ohno, and K. Ohtani, Electric-field control of ferromagnetism, Nature (London) **408**, 944 (2000).

[55] D. Chiba, M. Yamanouchi, F. Matsukura, and H. Ohno, Electrical Manipulation of Magnetization Reversal in a Ferromagnetic Semiconductor, Science **301**, 943 (2003).

[56] D. Chiba, A. Werpachowska, M. Endo, Y. Nishitani, F. Matsukura, T. Dietl, and H. Ohno, Anomalous Hall Effect in Field-Effect Structures of (Ga,Mn)As, Phys. Rev. Lett. **104**, 106601 (2010).

[57] T. Kurumaji, T. Nakajima, M. Hirschberger, A. Kikkawa, Y. Yamasaki, H. Sagayama, H. Nakao, Y. Taguchi, T.-h. Arima, Y. Tokura, Skyrmion lattice with a giant topological Hall effect in a frustrated triangular-lattice magnet. Science **365**,914-918 (2019).

[58] S.-G. Je, H.-S. Han, S. K. Kim, S. A. Montoya, W. Chao, I.-S. Hong, E. E. Fullerton, K.-S. Lee, K.-J. Lee, M.-Y. Im, and J.-I. Hong, Direct Demonstration of Topological Stability of Magnetic Skyrmions via Topology Manipulation. ACS Nano **14**, 3251-3258 (2020).

[59] A. Fert, N. Reyren, and V. Cros, Magnetic skyrmions: advances in physics and potential applications. Nature Reviews Materials **2**, 17031 (2017).

[60] N. Nagaosa, Y. Tokura, Topological properties and dynamics of magnetic skyrmions. Nature Nanotech. **8**, 899–911 (2013).

[61] P. Bruno, V. K. Dugaev, and M. Taillefumier, Phys. Rev. Lett. Topological Hall Effect and Berry Phase in Magnetic Nanostructures. **93**, 096806 (2004).

[62] L. Vistoli, W. Wang, A. Sander, Q. Zhu, B. Casals, R. Cichelero, A. Barthélémy, S. Fusil, G. Heranz, S. Valencia, R. Abrudan, E. Weschke, K. Nakazawa, H. Kohno, J. Santamaria, W. Wu, V. Garcia, M. Bibes, Giant Topological Hall Effect in Correlated Oxide Thin Films. Nat. Phys. **15**, 67−72 (2019).

[63] G. Kimbell, C. Kim, W. Wu, M. Cuoco, and J. W. A. Robinson, Challenges in identifying chiral spin textures via the topological Hall effect. Commun. Mater. **3**, 19 (2022).

[64] S. Mühlbauer, B. Binz, F. Jonietz, C. Pfleiderer, A. Rosch, A. Neubauer, R. Georgii, and P. Böni, Skyrmion Lattice in a Chiral Magnet. Science **323**, 915-919 (2009).

[65] A. Neubauer, C. Pfleiderer, B. Binz, A. Rosch, R. Ritz, P. G. Niklowitz, and P. Böni, Topological Hall Effect in the A Phase of MnSi. Phys. Rev. Lett. **102**, 186602 (2009).

[66] N. Kanazawa, Y. Onose, T. Arima, D. Okuyama, K. Ohoyama, S. Wakimoto, K. Kakurai, S. Ishiwata, and Y. Tokura, Large Topological Hall Effect in a Short-Period Helimagnet MnGe. Phys. Rev. Lett. **106**, 156603 (2011).

[67] S. X. Huang and C. L. Chien, Extended Skyrmion Phase in Epitaxial FeGe (111) Thin Films. Phys. Rev. Lett. **108**, 267201 (2012).

[68] K. Karube, J.S. White, D. Morikawa, M. Bartkowiak, A. Kikkawa, Y. Tokunaga, T. Arima, H.M. Rønnow, Y. Tokura, Y. Taguchi, Phys. Rev. Mater., **1** (2017).

[69] S. Sen, C. Singh, P. K. Mukharjee, R. Nath, and A. K. Nayak, Observation of the topological Hall effect and signature of room-temperature antiskyrmions in Mn-Ni-Ga D_{2d} Heusler magnets. Phys. Rev. B **99**, 134404 (2019).

[70] A. K. Nayak, V. Kumar, T. Ma, P. Werner, E. Pippel, R. Sahoo, F. Damay, U. K. Rößler, C. Felser, and S. S. P. Parkin, Magnetic antiskyrmions above room temperature in tetragonal Heusler materials. Nature **548**, 561 (2017).

[71] V. Kumar, N. Kumar, M. Reehuis, J. Gayles, A. S. Sukhanov, A. Hoser, F. Damay, C. Shekhar, P. Adler, and C. Felser, Detection of antiskyrmions by topological Hall effect in Heusler compounds. Phys. Rev. B **101**, 014424 (2020).

[72] P. Vir, J. Gayles, A. S. Sukhanov, N. Kumar, F. Damay, Y. Sun, J. K¨ubler, C. Shekhar, and C. Felser, Anisotropic topological Hall effect with real and momentum space Berry curvature in the antiskrymion-hosting Heusler compound $Mn_{1.4}PtSn$. Phys. Rev. B **99**, 140406 (2019).

[73] B. Giri, A. I. Mallick, C. Singh, P. V. P. Madduri, F. Damay, A. Alam, and A. K. Nayak, Robust topological Hall effect driven by tunable noncoplanar magnetic state in Mn-Pt-In inverse tetragonal Heusler alloys. Phys. Rev. B **102**, 014449 (2020).

[74] E. Skoropata, J. Nichols, J. M. Ok , R. V. Chopdekar, E. S. Choi, A. Rastogi, C. Sohn, X. Gao, S. Yoon, T. Farmer, R. D. Desautels, Y. Choi, D. Haskel, J. W. Freeland, S. Okamoto, M. Brahlek,and H. N. Lee, Interfacial tuning of chiral magnetic interactions for large topological Hall effects in $LaMnO_3/SrIrO_3$ heterostructures. Sci. Adv. **6**, eaaz3902 (2020).

[75] J. Matsuno , N. Ogawa , K. Yasuda, F. Kagawa, W. Koshibae, N. Nagaosa , Y. Tokura, M. Kawasaki, Interface-driven topological Hall effect in $SrRuO_3$-$SrIrO_3$ bilayer. Sci Adv **2**, e1600304 (2016).

[76] W. Wang, M. W. Daniels, Z. Liao, Y. Zhao, J. Wang, G. Koster, G. Rijnders, C.-Z. Chang, D. Xiao, and W. Wu, Spin chirality fluctuation in two-dimensional ferromagnets with perpendicular magnetic anisotropy. Nat Mater **18** 1054–9 (2019).

[77] A. Michels, D. Mettus, I. Titov, A. Malyeyev, M. Bersweiler, P. Bender, I. Peral, R. Birringer, Y. Quan, P. Hautle, J. Kohlbrecher, D. Honecker, J. R. Fernández, L. F. Barquín, and K. L. Met-

lov. Microstructural-defect-induced Dzyaloshinskii-Moriya interaction. Phys. Rev. B **99**, 014416 (2019).

[78] Y. Quan, J. Kohlbrecher, P. Hautle, and A. Michels, Defect-induced Dzyaloshinskii–Moriya interaction in a nanocrystalline two-phase alloy. J. Phys.: Condens. Matter **32** 285804 (2020).

[79] A. Crépieux, C. Lacroix, Dzyaloshinsky—Moriya interactions induced by symmetry breaking at a surface. J. Magn. Magn. Mater. **182** 341—349 (1998).

[80] R. A. Beck, L. Lu, P. V. Sushko, X. Xu, and X. Li, Defect-Induced Magnetic Skyrmion in a Two-Dimensional Chromium Triiodide Monolayer. J. Am. Chem. Soc. **1** 1362-1367 (2021).

[81] S.-Z. Lin, Skyrmion lattice in centrosymmetric magnets with local Dzyaloshinsky-Moriya interaction. arxiv (2021).

[82] W.-Y. Choi, W. Yoo, and M. H. Jung, Emergence of the topological Hall effect in a tetragonal compensated ferrimagnet $Mn_{2.3}Pd_{0.7}Ga$. NPG Asia Mater. **13**, 79 (2021).

[83] W. Wang, Y. Zhang, G. Xu, L. Peng, B. Ding, Y. Wang, Z. Hou, X. Zhang, X. Li, E. Liu, S. Wang, J. Cai, F. Wang, J. Li, F. Hu, G. Wu, B. Shen, and X.-X. Zhang, A Centrosymmetric Hexagonal Magnet with Superstable Biskyrmion Magnetic Nanodomains in a Wide Temperature Range of 100–340 K. Adv. Mater. **28**, 6887–6893 (2016).

[84] X. Xiao, L. Peng, X. Zhao, Y. Zhang, Y. Dai, J. Guo, M. Tong, J. Li, B. Li, W. Liu, J. Cai, B. Shen, and Z. Zhang, Low-field formation of room-temperature biskyrmions in centrosymmetric MnPdGa magnet. Appl. Phys. Lett. **114**, 142404 (2019).

[85] B. Göbel, I. Mertig, O. A. Tretiakov, Beyond skyrmions Review and perspectives of alternative magnetic quasiparticles. Physics Reports **895**, 1-28 (2021).

[86] Y. Tokura, and N. Kanazawa, Magnetic Skyrmion Materials. Chem Rev, **121**, 2857-2897 (2021).

[87] T. H. R. Skyrme, A UNIFIED FIELD THEORY OF MESONS AND BARYONS. Nuclear physics, (1962).

[88] A. Fert, V. Cros, and J. Sampaio, Skyrmions on the track. Nat Nanotechnol **8**, 152-156, (2013).

[89] U. K. Rossler, A. N. Bogdanov, and C. Pfleiderer, Spontaneous skyrmion ground states in magnetic metals. Nature **442**, 797-801, (2006).

[90] K. Yamada, S. Kasai, Y. Nakatani, K. Kobayashi, H. Kohno, A. Thiaville, and T. Ono, Electrical switching of the vortex core in a magnetic disk. Nat Mater **6**, 269-263, (2007).

[91] Z. Q. Liu, H. Chen, J. M. Wang, J. H. Liu, K. Wang, Z. X. Feng, H. Yan, X. R. Wang, C. B. Jiang, J. M. D. Coey, A. H. MacDonald, Electrical switching of the topological anomalous Hall effect in a non-collinear antiferromagnet above room temperature. Nat. Electron. **1**, 172 (2018).

[92] H. Wang, Y. Dai, G.-M. Chow, J. Chen, Topological hall transport: Materials, mechanisms and potential applications, Progress in Materials Science **130**, 100971 (2022).

[93] C. Sürgers, G. Fischer, P. Winkel, and H. v. Löhneysen, Large topological Hall effect in the non-collinear phase of an antiferromagnet. Nat. Commun. **5**, 3400 (2014).
via the topological Hall effect. Commun. Mater. **3**, 19 (2022).

[94] Z. H. Liu, Y. J. Zhang, G. D. Liu, B. Ding, E. K. Liu, H. M. Jafri, Z. P. Hou, W. H. Wang, X. Q. Ma, and G. H. Wu, Transition from Anomalous Hall Effect to Topological Hall Effect in Hexagonal Non-Collinear Magnet Mn_3Ga. Sci Rep **7**, 515 (2017).

[95] P. K. Rout, P. V. P. Madduri, S. K. Manna, and A. K. Nayak, Field-induced topological Hall effect in the noncoplanar triangular antiferromagnetic geometry of Mn_3Sn. Phys. Rev. B **99**, 094430 (2019).

[96] Y. Shiomi, M. Mochizuki, Y. Kaneko, and Y. Tokura, Hall Effect of Spin-Chirality Origin in a Triangular-Lattice Helimagnet $Fe_1.3Sb$. Phys. Rev. Lett. **108**, 056601 (2012).

[97] J. Liu, S. Zuo, X. Zheng, Y. Zhang, T. Zhao, F. Hu, J. Sun, B. Shen, Magnetic transition behavior and large topological Hall effect in hexagonal $Mn_{2-x}Fe_{1+x}Sn$ (x=0.1) magnet. Appl. Phys. Lett. **117**, 052407 (2020).

[98] J. Liu, S.L. Zuo, J. Shen, Y. Zhang, Y. Zhang, Z.X. Li, X.Q. Gao, H.F. Kang, T.Y. Zhao, F.X. Hu, J. Sun and B.G. Shen, Large topological Hall effect and in situ observation of magnetic domain structures in the Mn_2FeSn compound. Mater. Today Phys. **29**, 100871 (2022).

[99] V. Kumar, G. K. Shukla, N. Shahi, S. Singh, Topological Hall Effect in $(Mn_{1-x}Fe_x)_{3.25}Ge$ (x = 0.4) Hexagonal Magnet. Phys. Status Solidi RRL 2300174 (2023).

[100] N. J. Ghimire, R. L. Dally, L. Poudel, D. C. Jones, D. Michel, N. T. Magar, M. Bleuel, M. A. McGuire, J. S. Jiang, J. F. Mitchell, J. W. Lynn and I. I. Mazin, Competing magnetic phases and fluctuation-driven scalar spin chirality in the kagome metal YMn_6Sn_6. Sci. Adv. **6**, eabe2680 (2020).

[101] Y. Taguchi, Y. Oohara, H. Yoshizawa, N. Nagaosa, T. Sasaki, S. Awaji, Y. Iwasa, T. Tayama, T. Sakakibara, S. Iguchi, K. Ohgushi, T. Ito, The spin chirality induced anomalous Hall effect in pyrochlore ferromagnets. J. Phys: Condens. Matter. **16** S599–606 (2004).

[102] J. Jiang, D. Xiao, F. Wang, J.-H. Shin, D. Andreoli, J. Zhang, R. Xiao, Y.-F. Zhao, M. Kayyalha, L. Zhang, K. Wang, J. Zang, C. Liu, N. Samarth, M. H. W. Chan, and C.-Zu Chang, Concurrence of quantum anomalous Hall and topological Hall effects in magnetic topological insulator sandwich heterostructures. Nat. Mater. **19**, 732–737 (2020).

[103] M. Yokoi, S. Fujiwara, T. Kawamura, T. Arakawa, K. Aoyama, H. Fukuyama, K. Kobayashi, and Y. Niimi, Negative resistance state in superconducting NbSe2 induced by surface acoustic waves. Sci. Adv. **6**,eaba1377 (2020).

[104] D. Khadka, T. R. Thapaliya, S. H. Parra, X. Han, J. Wen, R. F. Need, P. Khanal, W. Wang, J. Zang, J. M. Kikkawa, L. Wu, S. X. Huang, Kondo physics in antiferromagnetic Weyl semimetal $Mn_{3+x}Sn_{1-x}$ films, Sci. Adv. , **6** 1-8 (2020).

[105] O. Breunig, Z. Wang, A. Taskin, J. Lux, A. Rosch, and Y. Ando, Gigantic negative magnetoresistance in the bulk of a disordered topological insulator. Nat. Commun. **8**, 15545 (2017).

[106] L. Liang, Field effect controlled magnetism and magnetotransport in low dimensions. [Thesis fully internal (DIV), University of Groningen]. Rijksuniversiteit Groningen (2017).

[107] R. J. D. Tilley, Understanding Solids: The Science of Materials, John Wiley and Sons Ltd., London, 395 (2004).

[108] A. Matthiessen and C. Vogt, On the Influence of Temperature on the Electric Conducting Power of Alloys, Philos. Trans. R. Soc. Lond., **154** 167–200 (1864).

[109] A. Matthiessen and C. Vogt, On the Influence of Temperature on the Electric Conducting Power of Thallium and Iron, Philos. Trans. R. Soc. Lond., **153** 369–383 (1863).

[110] N. Wiser, The electrical resistivity of the simple metals, Contemp. Phys., **25** 211-249 (2006).

[111] https://en.wikipedia.org/wiki/Superconductivity

[112] W. J. de Haas, J. de Boer, and G. J. van dën berg, The electrical resistance of gold, copper and lead at low temperatures, Physica, **1** 1115-1124 (1934).

[113] G.J. van den Berg, Anomalies in dilute metallic solutions of transitions metals J. G. Daunt, D. O. Edwards, F. J. Milford, and M. Yaqub (eds) Low Temperature Physics LT**9**, (1965) 955–984.

[114] J. Kondo, Resistance Minimum in Dilute Magnetic Alloys, Prog. Theor. Phys., **32** 37-49 (1964).

[115] P.W. Anderson, Localized Magnetic States in Metals, Phys. Rev., **124** 41-53 (1961).

[116] L. Kouwenhoven and L. Glazman, Revival of the Kondo effect, Physics World **14** 33 (2001).

[117] scholarpedia.org/article/Kondoeffect

[118] X. Ding, J. Xing, G. Li, L. Balicas, K. Gofryk, and H.-H. Wen, Crossover from Kondo to Fermi-liquid behavior induced by high magnetic field in 1T − VTe_2 single crystals. Phys. Rev. B **103**, 125115 (2021).

[119] L. Zhu, G. Woltersdorf, and J. Zhao, Observation of orbital two-channel Kondo effect in a ferromagnetic L10-MnGa film. Sci. Rep. **6**, 34549 (2016).

[120] L. Yu, S. Y.-Tao, Y. Y.-Feng, Theoretical progress and material studies of heavy fermion superconductors, Acta Physica Sinica **70** 017402-1-017402-31 (2021).

[121] H. Watanabe, M. Ogata, Crossover from dilute-Kondo system to heavy-fermion system, Phys. Rev. B, **81** 113111 (2010).

[122] F.C. Ragel, P.d.V. du Plessis, A.M. Strydom, Effects of La dilution on the $CePt_2Si_2$ Kondo lattice, J. Phys. Condens. Matter, **20** 055218 (2008).

[123] J. Chen, Z. Wang, S. Zheng, C. Feng, J. Dai, Z. Xu, Antiferromagnetic Kondo lattice compound $CePt_3P$, Sci. Rep., **7** 41853 (2017).

[124] A. Generalov, D.A. Sokolov, A. Chikina, Y. Kucherenko, V.N. Antonov, L.V. Bekenov, S. Patil, A.D. Huxley, J.W. Allen, K. Matho, K. Kummer, D.V. Vyalikh, C. Laubschat, Insight into the temperature dependent properties of the ferromagnetic Kondo lattice YbNiSn, Phys. Rev. B, **95** 184433 (2017).

[125] A. M. Tsveliek, P.B. Wiegmann, Exact Solution of the Multichannel Kondo Problem, Scaling, and Integrability. J. Stat. Phys., **38** 125-147 (1985).

[126] A. A. Zvyagin, P. Schlottmann, Finite-size effects in a metallic multichannel ring with Kondo impurity Persistent currents and magnetoresistance, Phys. Rev. B, **54** 15191 (1996).

[127] K. R. Sapkota, F. S. Maloney, W. Wang, Observations of the Kondo effect and its coexistence with ferromagnetism in a magnetically undoped metal oxide nanostructure, Phys. Rev. B, **97** 144425 (2018).

[128] J.-H. Chen, L. Li, W. G. Cullen, E. D. Williams, M. S. Fuhrer, Tunable Kondo effect in graphene with defects, Nat. Phys., **7** 535-538 (2011).

[129] A. Zrenner, L.V. Butov, M. Hagn, G. Abstreiter, G. Bohm, G. Weimann, Quantum dots formed by interface fluctuations in AlAs/GaAs coupled quantum well structures, Phys. Rev. Lett., **72** 3382-3385 (1994).

[130] R.R. Nair, I.L. Tsai, M. Sepioni, O. Lehtinen, J. Keinonen, A.V. Krasheninnikov, A.H. Castro Neto, M.I. Katsnelson, A.K. Geim, I.V. Grigorieva, Dual origin of defect magnetism in graphene and its reversible switching by molecular doping. Nat. Commun., **4** 2010 (2013).

[131] S. Seiro, L. Jiao, S. Kirchner, S. Hartmann, S. Friedemann, C. Krellner, C. Geibel, Q. Si, F. Steglich, and S. Wirth, Evolution of the Kondo lattice and non-Fermi liquid excitations in a heavy-fermion metal. Nat. Commun., **9** 3324 (2018).

[132] S. Kobayashi, Y. Yoshino, S. Tsuji, S. Masafumi, F. Iga, Kondo Effect in the Long-Range Antiferromagnetic Ordered State –$Ce_xNd_{1-x}B_6$–. J. Phys. Soc. Japan, **72** 25-28 (2003).

[133] H.H. Lai, S.E. Grefe, S. Paschen, Q. Si, Weyl-Kondo semimetal in heavy-fermion systems, Proc. Natl. Acad. Sci. U. S. A., **115** 93-97 (2018).

[134] A. Maurya, R. KulkarniA. Thamizhavel, D. Paudyal and S. K. Dhar, Kondo Lattice and Antiferromagnetic Behavior in Quaternary $CeTAl_4Si_2$ (T = Rh, Ir) Single Crystals, J. Phys. Soc. Japan, **85** 034720 (2016).

[135] D. K. Singh, A. Thamizhavel, J. W. Lynn, S. Dhar, J. Rodriguez-Rivera, T. Herman, , Field-induced quantum fluctuations in the heavy fermion superconductor CeCu(2)Ge(2), Sci. Rep., **1** 117 (2011).

[136] G. Zwicknagl, Kondo Effect and Antiferromagnetism in $CeCu_2Ge_2$: An Electronic Structure Study, J. Low Temp. Phys., **147** 123-134 (2007).

[137] O. Stockert, F. Steglich, Unconventional Quantum Criticality in Heavy-Fermion Compounds. Annu. Rev. Condens. Matter Phys., **2** 79-99 (2011).

[138] J. Wang, Y.-f. Yang, Nonlocal Kondo effect and quantum critical phase in heavy-fermion metals. Phys. Rev. B, **104** 165120 (2021).

[139] S. Nakatsuji, K. Kuga, Y. Machida, T. Tayama, T. Sakakibara, Y. Karaki, H. Ishimoto, S. Yonezawa, Y. Maeno, E. Pearson, G.G. Lonzarich, L. Balicas, H. Lee, Z. Fisk, Superconductivity and quantum criticality in the heavy-fermion system β-$YbAlB_4$. Nat. Phys., **4** 603-607 (2008).

[140] K. R. Shirer, A. C. Shockley, A. P. Dioguardi, J. Crocker, C. H. Lin, N. apRoberts-Warren, D. M. Nisson, P. Klavins, J. C. Cooley, Y.-f. Yang, and N. J. Curro, Long range order and two-fluid behavior in heavy electron materials, Proc. Natl. Acad. Sci. USA **109**, E3067 (2012).

[141] A. R. Paul, M. Mukherjee, D. Singh, A Critical Review on the Properties of Intermetallic Compounds and Their Application in the Modern Manufacturing. Crystal Research and Technology. **57**, 2100159 (2022).

[142] https://en.wikipedia.org/wiki/Intermetallic

[143] X. Zhou, J.-P. Hanke, W. Feng, S. Blügel, Y. Mokrousov, and Y. Yao, Giant anomalous Nernst

effect in noncollinear antiferromagnetic Mn-based antiperovskite nitrides. Phys. Rev. Materials **4**, 024408 (2020).

[144] S. Singh, R. Rawat, S. E. Muthu, S. W. D'Souza, E. Suard, A. Senyshyn, S. Banik, P. Rajput, S. Bhardwaj, A. M. Awasthi, R. Ranjan, S. Arumugam, D. L. Schlagel, T. A. Lograsso, A. Chakrabarti, and S. R. Barman, Spin-Valve-Like Magnetoresistance in Mn_2NiGa at Room Temperature. Phys. Rev. Lett. **109**, 246601 (2012).

[145] J. Zemen, E. Mendive-Tapia, Z. Gercsi, R. Banerjee, J. B. Staunton, and K. G. Sandeman, Frustrated magnetism and caloric effects in Mn-based antiperovskite nitrides: Ab initio theory. Phys. Rev. B **95**, 184438 (2017).

[146] D. Matsunami, A. Fujita, K. Takenaka, M. Kano, Giant barocaloric effect enhanced by the frustration of the antiferromagnetic phase in Mn_3GaN, Nat. Mater., **14** 73-78 (2015).

[147] K. Shi, Y. Sun, J. Yan, S. Deng, L. Wang, H. Wu, P. Hu, H. Lu, M. I. Malik, Q. Huang, and C. Wang, Baromagnetic Effect in Antiperovskite $Mn3Ga_{0.95}N_{0.94}$ by Neutron Powder Diffraction Analysis. Adv. Mater. **28**, 3761- 3767 (2016).

[148] Z. Y. Liu, Q. X. Dong, P. T. Yang, P. F. Shan, B. S. Wang, J. P. Sun, Z. L. Dun, Y. Uwatoko, G. F. Chen, X. L. Dong, Z. X. Zhao, and J.-G. Cheng, Pressure-Induced Superconductivity up to 9 K in the Quasi-One-Dimensional KMn_6Bi_5 Phys. Rev. Lett. **128**, 187001 (2022).

[149] F. Heusler, Ueber magnetische Manganlegierungen. Verh. Dtsch. Phys. Ges. **5** 219 (1903).

[150] F. Heusler, W. Starck, E. Haupt, Magnetisch-chemische Studien. Verh. Dtsch. Phys. Ges. **5** 220 (1903).

[151] T. Graf, C. Felser, and S. S. P. Parkin, Simple rules for the understanding of Heusler compounds. Prog. Solid. State Ch. **39**, 1-50 (2011).

[152] L. Wollmann, A. K. Nayak, S. S. P.Parkin, and C. Felser, Heusler 4.0: Tunable Materials. Annu. Rev. Mater. Res. **47**, 247-270 (2017).

[153] K. Manna, Y. Sun, L. Muechler, J. Kübler, and C. Felser, Heusler, Weyl and Berry. Nat. Rev. Mater. **3**, 244–256 (2018).

[154] F. Casper, T. Graf, S. Chadov, B. Balke, and C. Felser, Half-Heusler compounds: novel materials for energy and spintronic applications. Semicond. Sci. Technol. **27**, 063001 (2012).

[155] E. V. Vidal, G. Stryganyuk, H. Schneider, C. Felser, and G. Jakob, Exploring Co_2MnAl Heusler compound for anomalous Hall effect sensors. Appl. Phys. Lett. **99**, 132509 (2011).

[156] G. K. Shukla, A. K. Jena, N. Shahi, K. K. Dubey, I. Rajput, S. Baral, K. Yadav, K. Mukherjee , A. Lakhani, K. Carva, S.-C. Lee, S. Bhattacharjee, and S. Singh, Atomic disorder and Berry phase driven anomalous Hall effect in a Co_2FeAl Heusler compound. Phys. Rev. B **105**, 035124 (2022).

[157] N. Shahi, A. K. Jena, G. K. Shukla, V. Kumar, S. Rastogi, K. K. Dubey, I. Rajput, S. Baral, A. Lakhani, S.-C. Lee, S. Bhattacharjee, and S. Singh, Antisite disorder and Berry curvature driven anomalous Hall effect in the spin gapless semiconducting Mn_2CoAl Heusler compound. Phys. Rev. B **106**, 245137 (2022).

[158] K. Manna, L. Muechler, T.-H. Kao, R. Stinshoff, Y. Zhang, J. Gooth, N. Kumar, G. Kreiner, K. Koepernik, R. Car, J. Kübler, G. H. Fecher, C. Shekhar, Y. Sun, and C. Felser, From Colossal to Zero: Controlling the Anomalous Hall Effect in Magnetic Heusler Compounds via Berry Curvature Design. Phys. Rev. X **8**, 041045 (2018).

[159] J. Shen, Q. Yao, Q. Zeng, H. Sun, X. Xi, G. Wu, W. Wang, B. Shen, Q. Liu, and E. LiuLocal, Disorder-Induced Elevation of Intrinsic Anomalous Hall Conductance in an Electron-Doped Magnetic Weyl Semimetal. Phys. Rev. Letter. **125**, 086602 (2020).

[160] K. Hu, R. Xie, C. Shen, H. Penga, H. Liua, and H. Zhang, High-Throughput Design of Co-Based Magnetic Heusler Compounds (2023)

[161] P. Li, J. Koo, W. Ning, J. Li, L. Miao, L. Min, Y. Zhu, Y. Wang, N. Alem, C.-X. Liu, Z. Mao, and B. Yan, Giant room temperature anomalous Hall effect and tunable topology in a ferromagnetic topological semimetal Co_2MnAl. Nat. Commun. **11**, 3476 (2020).

[162] S. Roy, R. Singha, A. Ghosh, A. Pariari, and P. Mandal, Phys. Rev. B **102**, 085147 (2020).

[163] F. Mende, J. Noky, S. N. Guin, G. H. Fecher, K. Manna, P. Adler, W. Schnelle, Y. Sun, C. Fu,

and C. Felser, Large Anomalous Hall and Nernst Effects in High Curie-Temperature Iron-Based Heusler Compounds. Adv. Sci. **8**, 2100782 (2021).

[164] T. Graf, C. Felser, S. S. P. Parkin, Heusler Compounds: Applications in Spintronics. Handbook of Spintronics, ISBN : 978-94-007-6891-8 (2016).

[165] D. Rani, L. Bainsla, A. Alam, K. G. Suresh, Spin-gapless semiconductors: Fundamental and applied aspects. J. Appl. Phys. **128** (22) 220902 (2020).

[166] X. Wang, Z. Cheng, G. Zhang, H. Yuan, H. Chen, X.-L. Wang, Spin-gapless semiconductors for future spintronics and electronics. Phys. Rep. **888**, (2020).

[167] I. Dubenko, T. Samanta, A. K. Pathak, A. Kazakov, V. Prudnikov, S. Stadler, A. Granovsky, A. Zhukov, N. Ali, Magnetocaloric effect and multifunctional properties of Ni–Mn-based Heusler alloys. **324** 3530-3534 (2012).

[168] S. Singh, B. Dutta, S. W. D Souza, M. G. Zavareh, P. Devi, A. S. Gibbs, T. Hickel, S. Chadov, C. Felser, and D. Pandey. Robust Bain distortion in the premartensite phase of a platinum-substituted Ni_2MnGa magnetic shape memory alloy. Nat. Commun. **8**, 1006 (2017).

[169] J. Kübler, A. R. Williams, and C. B. Sommers, Formation and coupling of magnetic moments in Heusler alloys. Phys. Rev. B **38**, 1745-1755 (1983).

[170] G. D. Liu, X. F. Dai, S. Y. Yu, Z. Y. Zhu, J. L. Chen, and G. H. Wu, Physical and electronic structure and magnetism of Mn_2NiGa: Experiment and density-functional theory calculations. Phys. Rev. B **74**, 054435 (2006).

[171] G. D. Liu, J. L. Chen, Z. H. Liu, X. F. Dai, and G. H. Wu, Martensitic transformation and shape memory effect in a ferromagnetic shape memory alloy: Mn_2NiGa. Appl. Phys. Lett. **87**, 262504 (2005).

[172] A. K. Singh, G. K. Shukla, and S. Singh, Intrinsic anomalous Hall conductivity and real space Berry curvature induced topological Hall effect in Ni_2MnGa magnetic shape memory alloy. J. Phys. D: Appl. Phys. **56**, 044004 (2023).

[173] Y. Xie, J. Ma, H. Vakilitaleghani, Y. Tan, and A. W. Ghosh, Computational Search for Ul-

trasmall and Fast Skyrmions in the Inverse Heusler Family. IEEE Trans. Magn., **56**, 1500108 (2020).

[174] Z.H. Liu and A. Burigu and Y.J. Zhang and Hasnain Mehdi Jafri and X.Q. Ma and E.K. Liu and W.H. Wang and G.H. Wu, Giant topological Hall effect in tetragonal Heusler alloy Mn_2PtSn. Scr. Mater. **143** 122-125 (2018).

[175] M. Meinert, J.-M. Schmalhorst, and G. Reiss, Exchange interactions and Curie temperatures of Mn_2CoZ compounds. J. Phys.: Condens. Matter **23**, 116005 (2011).

[176] A. Jakobsson, P. Mavropoulos, E. Şaşıoğlu, S. Blügel, M. Ležaić, B. Sanyal, and I. Galanakis, First-principles calculations of exchange interactions, spin waves, and temperature dependence of magnetization in inverse-Heusler-based spin gapless semiconductors. Phys. Rev. B **91**, 174439 (2015).

[177] A. Kundu, S. Ghosh, R. Banerjee, S. Ghosh, and B. Sanyal, New quaternary half-metallic ferromagnets with large Curie temperatures. Sci Rep **7**, 1803 (2017).

[178] Z. Yue, Z. Li, L. Sang, and X. Wang, Spin-Gapless Semiconductors. Small **16** 1905155 (2020).

[179] X. L. Wang, Proposal for a New Class of Materials: Spin Gapless Semiconductors, Phys. Rev. Lett., **100**, 156404 (2008).

[180] Z. Z. Abidin, P. T. Mativenga, and G. Harrison, Chilled Air System and Size Effect in Micro-milling of Nickel−Titanium Shape Memory Alloys. Int. J. of Precis. Eng. and Manuf.-Green Tech. **7**, 283–297 (2020).

[181] V. V. Marchenkov, V. Y.Irkhin, and A. A. Semiannikova, Unusual Kinetic Properties of Usual Heusler Alloys. J Supercond. Nov. Magn. **35**, 2153–2168 (2022).

[182] R. Masrour, A. Jabar, L. Bahmad, E. K. Hlil, M. Hamedoun, A. Benyoussef, A. Hourmatallah, N. Benzakour, A. Rezzouk, K. Bouslykhane, Magnetic Properties of Mn_3ZnN Anti-perovskite Nanoparticles: A Monte Carlo Simulations. J. Clust. Sci. **32**, 163–166 (2021).

[183] https://en.wikipedia.org/wiki/Pnictogen

[184] X. Chong, Y. Jiang, R. Zhou, and Jing Feng, Pressure dependence of electronic structure and superconductivity of the MnX (X= N, P, As, Sb). Sci. Rep. **6**, 21821 (2016).

[185] O. Rader, A. Kimura, N. Kamakura, K.-S. An, A. Kakizaki, S. Miyanishi, H. Akinaga, M. Shirai, K. Shimada, and A. Fujimori, Exchange splittings of Mn- and Sb-derived states by spin-resolved valence-band photoemission of MnSb. Phys. Rev. B **57**, R689–R692 (1998).

[186] A. Continenza, S. Picozzi, W. T. Geng, and A. J. Freeman, Coordination and chemical effects on the structural, electronic, and magnetic properties in Mn pnictides. Phys. Rev. B **64** 085204 (2001).

[187] R. Masrour, E. K. Hlil, M. Hamedoun, A. Benyoussef, O. Mounkachi and H. E. Moussaoui, Electronic and Magnetic Properties of MnSb Compounds. J. Supercon. Novel Magn. **28**, 1815-1819 (2015).

[188] L.N. Oveshnikov, A.B. Granovsky, A.B. Davydov, A.V. Bogach, A.M. Kharlamova, A.I. Ril', B.A. Aronzon, Magnetic and magnetotransport properties of MnSb polycrystals near equatomic composition. J. Magn. Magn. Mater **563**, 169873 (2022).

[189] S. F. Marenkin, A. V. Kochura, A. D. Izotov, M. G. Vasil'ev, Manganese Pnictides MnP, MnAs, and MnSb are Ferromagnetic Semimetals: Preparation, Structure, and Properties (a Survey). Russ. J. Inorg. Chem. **63(14)**, 1753–1763 (2018).

[190] Y. Choi, P. J. Ryan, M. A. McGuire, B. C. Sales, J.-W. Kim, Giant magnetostriction effect near onset of spin reorientation in MnBi. Appl. Phys. Lett. **112**, 192411 (2018).

[191] https://en.wikipedia.org/wiki/Antiperovskite

[192] C. X. Quintela, K. Song, D.-F. Shao, L. Xie, T. Nan, T. R. Paudel, N. Campbell, X. Pan, T. Tybell, M. S. Rzchowski, E. Y. Tsymbal, S.-Y. Choi, C.-B. Eom, Epitaxial antiperovskite/perovskite heterostructures for materials design. Sci. Adv. **6**, eaba4017 (2020).

[193] H.K. Singh, I. Samathrakis, N.M. Fortunato, J. Zemen, C. Shen, O. Gutfleisch, H. Zhang, Multifunctional antiperovskites driven by strong magnetostructural coupling. npj Comput. Mater. **7**, 98 (2021).

[194] D.-F. Shao, G. Gurung, T.R. Paudel, E.Y. Tsymbal, Electrically reversible magnetization at the antiperovskite/perovskite interface. Phys. Rev. Mater. **3**, 024405 (2019).

[195] P. Lukashev, K.D. Belashchenko, R.F. Sabirianov, Large magnetoelectric effect in ferroelectric/piezomagnetic heterostructures. Phys. Rev. B **84**, 134420 (2011).

[196] K. Kamishima, T. Goto, H. Nakagawa, N. Miura, M. Ohashi, N. Mori, T. Sasaki, T. Kanomata, Giant magnetoresistance in the intermetallic compound Mn_3GaC. Phys. Rev. B **63**, 024426 (2000).

[197] K. Asano, K. Koyama, K. Takenaka, Magnetostriction in Mn_3CuN, Appl. Phys. Lett. **92**, 161909 (2008).

[198] K. Takenaka, T. Shibayama, D. Kasugai, T. Shimizu, Giant Field-Induced Distortion in Mn_3SbN at Room Temperature, Jpn. J. Appl. Phys. **51**, 043001 (2012).

[199] T. Tohei, H. Wada, T. Kanomata, Negative magnetocaloric effect at the antiferromagnetic to ferromagnetic transition of Mn_3GaC, J. Appl. Phys. **94**, 1800-1802 (2003).

[200] B. S. Wang, P. Tong, Y. P. Sun, X. Luo, X. B. Zhu, G. Li, X.D. Zhu, S.B. Zhang, Z. R. Yang, W. H. Song, J. M. Dai, Large magnetic entropy change near room temperature in antipervoskite $SnCMn_3$. EPL (Europhys. Lett.) **85**, 47004 (2009).

[201] J. Zheng, B. Perry, Y. Wu, Antiperovskite Superionic Conductors: A Critical Review. ACS Materials Au **1**, 92-106 (2021).

[202] Y. Zhao, L.L. Daemen, Superionic conductivity in lithium-rich anti-perovskites. J. Am. Chem. Soc. **134**, 15042-15047 (2012).

[203] H. Fanga and P. Jenaa, Li-rich antiperovskite superionic conductors based on cluster ions. Proc. Natl. Acad. Sci. **114**, 11046-11051 (2017).

[204] T. He, Q. Huang, A. P. Ramirez, Y. Wang, K. A. Regan, N. Rogado, M. A. Hayward, M. K. Haas, J. S. Slusky, K. Inumara, H. W. Zandbergen, N. P. Ong and R. J. Cava, Superconductivity in the non-oxide perovskite $MgCNi_3$. Nat. lett. **411**, 54-56 (2001).

[205] M. Uehara, A. Uehara, K. Kozawa, Y. Kimishima, New Antiperovskite-Type Superconductor $ZnNyNi_3$. J. Phys. Soc. Japan **78**, 033702 (2009).

[206] K. Takenaka, H. Takagi, Giant negative thermal expansion in Ge-doped anti-perovskite manganese nitrides. Appl. Phys. Lett. **87**, 261902 (2005).

[207] K. Takenaka, T. Hamada, D. Kasugai, N. Sugimoto, Tailoring thermal expansion in metal matrix composites blended by antiperovskite manganese nitrides exhibiting giant negative thermal expansion. J. Appl. Phys. **112**, 083517 (2012).

[208] R. Huang, L. Li, F. Cai, X. Xu, L. Qian, Low-temperature negative thermal expansion of the antiperovskite manganese nitride Mn_3CuN codoped with Ge and Si. Appl. Phys. Lett. **93**, 081902 (2008).

[209] J. Tan, R. Huang, W. Wang, W. Li, Y. Zhao, S. Li, Y. Han, C. Huang, L. Li, Broad negative thermal expansion operation-temperature window in antiperovskite manganese nitride with small crystallites. Nano Res. **8**, 2302-2307 (2015).

[210] Y. Zhu, G. Chen, Y. Zhong, Y. Chen, N. Ma, W. Zhou, Z. Shao, A surface-modified antiperovskite as an electrocatalyst for water oxidation. Nat. Commun. **9**, 2326 (2018).

[211] P.F. Li, Y.Y. Tang, W.Q. Liao, P.P. Shi, X.N. Hua, Y. Zhang, Z. Wei, H. Cai, R.G. Xiong, Experimental Evidence for a Triboluminescent Antiperovskite Ferroelectric: Tris(trimethylammonium) catena-Tri-mu-chloro-manganate(II) Tetrachloromanganate(II). Angew Chem Int Ed Engl **57**, 11939-11942 (2018).

[212] Z. Yu, H. Peng, Q. Wei, T. Huang, S. Yao, Y. Tian, C. Peng, B. Zou, The magnetic polaron modulated luminescence bands of organic-inorganic hybrid ferroelectric anti-perovskite $(C_3H_9N)_3Cd_2C_l7$ doped with Mn^2+. Mater. Today Chem. **24**, 100781 (2022).

[213] B.Y. Qu, B.C. Pan, Nature of the negative thermal expansion in antiperovskite compound Mn_3ZnN. J. Appl. Phys.**108**, 113920 (2010).

[214] T. Hamada, K. Takenaka, Giant negative thermal expansion in antiperovskite manganese nitrides. J. Appl. Phys. **109**, 07E309 (2011).

[215] H. Lu, Y. Sun, K. Shi, J. Cui, H. Han, C. Wang, Negative thermal expansion, magnetic and electronic transport properties in antiperovskite compounds $Mn_3Ga_{1-x}Ag_xN$ ($0 \leq x \leq 1.0$). J. Magn. Magn. Mater. **514**, 167137 (2020).

[216] S. Tan, C. Gao, C. Wang, T. Zhou, G. Yin, M. Sun, F. Xing, R. Cao, Y. Sun, The tunable negative thermal expansion covering a wide temperature range around room temperature in Sn, Mn co-substituted Mn(3)ZnN. Dalton. Trans. **49**, 10407-10412 (2020).

[217] K. Takenaka, M. Ichigo, T. Hamada, A. Ozawa, T. Shibayama, T. Inagaki, K. Asano, Magnetovolume effects in manganese nitrides with antiperovskite structure. Sci. Technol. Adv. Mater., **15** 015009 (2014).

[218] D. Boldrin, I. Samathrakis, J. Zemen, A. Mihai, B. Zou, F. Johnson, B.D. Esser, D.W. McComb, P.K. Petrov, H. Zhang, L.F. Cohen, Anomalous Hall effect in noncollinear antiferromagnetic Mn_3NiN thin films, Phys. Rev. Mater. **3**, 094409 (2019).

[219] K. Zhao, T. Hajiri, H. Chen, R. Miki, H. Asano, P. Gegenwart, Anomalous Hall effect in the noncollinear antiferromagnetic antiperovskite $Mn_3Ni_{1-x}Cu_xN$, Phys. Rev. B **100**, 045109 (2019).

[220] G. Gurung, D.-F. Shao, T.R. Paudel, E.Y. Tsymbal, Anomalous Hall conductivity of noncollinear magnetic antiperovskites. Phys. Rev. Mater. **3**, 044409 (2019).

[221] D. Huang, H. Li, X. Xi, J. Gao, Y.C. Lau, W. Wang, Magnetoresistance reversals and anomalous Hall effect in Mn(3)SnC and effects of carbon deficiency, J. Phys. Condens. Matter. **35**, 025702 (2023).

[222] Y. You, H. Lam, C. Wan, C. Wan, W. Zhu, L. Han, H. Bai, Y. Zhou, L. Qiao, T. Chen, F. Pan, J. Liu, C. Song, Anomalous Nernst Effect in an Antiperovskite Antiferromagnet. Phys. Rev. Appl. **18**, 024007 (2022).

[223] T. Hajiri, K. Matsuura, K. Sonoda, E. Tanaka, K. Ueda, H. Asano, Spin-Orbit-Torque Switching of Noncollinear Antiferromagnetic Antiperovskite Manganese Nitride Mn_3GaN, Phys. Rev. Appl. **16**, 024003 (2021).

[224] B. H. Rimmler, B. K. Hazra, B. Pal, K. Mohseni, J. M. Taylor, A. Bedoya-Pinto, H. Deniz, M. Tangi, I. Kostanovskiy, C. Luo, R. R. Neumann, A. Ernst, F. Radu, I. Mertig, H. L. Meyerheim,

and S. S. P. Parkin, Atomic Displacements Enabling the Observation of the Anomalous Hall Effect in a Non-Collinear Antiferromagnet. Adv. Mater. **35**, 2209616 (2023).

[225] J-P. Jardin, J. Labbe, Phase transitions and band structure in metallic perovskites (carbides and nitrides), J. Solid State Chem. **46** 275-293 (1983).

[226] R. Navarro, J.A. Rojo, Spin-Glass-Like Phase in $Mn_{4-x}Ga_xN$ Solid Solution, Magnetic Properties for x = 0.75, 0.85, 0.9, 0.95 and 1.0, J. Magn. Magn. Mater., **59** 221-234 (1986).

[227] K. Arima, F. Kuroda, S. Yamada, T. Fukushima, T. Oguchi, and K. Hamaya, Anomalous Hall conductivity and electronic structures of Si-substituted Mn_2CoAl epitaxial films, Phys. Rev. B **97**, 054427 (2018).

[228] R. G. Buckley, T. Butler, C. Pot, N. M. Strickland and S. Granville, Exploring disorder in the spin gapless semiconductor Mn_2CoAl, Mater. Res. Express **6**, 106113 (2019).

[229] W. Zhang, B. Balasubramanian, A. Ullah, R. Pahari, X. Li, L. Yue, S. R. Valloppilly, A. Sokolov, R. Skomski, and D. J. Sellmyer, Comparative study of topological Hall effect and skyrmions in NiMnIn and NiMnGa. Appl. Phys. Lett. **115**, 172404 (2019).

[230] Y. He, S. Schneider, T. Helm, J. Gayles, D. Wolf, I. Soldatov, H. Borrmann, W. Schnelle, R. Schaefer, G. H. Fecher, B. Rellinghaus, C. Felser, Topological Hall effect arising from the mesoscopic and microscopic non-coplanar magnetic structure in MnBi. Acta. Mater. **226**, 117619 (2022).

[231] S. Ouardi, G. Fecher, C. Felser, and J. Kübler, Realization of Spin Gapless Semiconductors: The Heusler Compound Mn_2CoAl, Phys. Rev. Lett. **110**, 100401 (2013).

[232] X. D. Xu, Z. X. Chen, Y. Sakuraba, A. Perumal, K. Ma-suda, L. S. R. Kumara, H. Tajiri, T. Nakatani, J. Wang, W. Zhou, Y. Miura, T. Ohkubo, and K. Hono, Microstructure, magnetic and transport properties of a Mn_2CoAl Heusler compound, Acta Mater. **176**, 33-42 (2019).,

[233] P. Chen, C. Gao, G. Chen, K. Mi, M. Liu, P. Zhang, and D. Xue, The low-temperature transport properties of Heusler alloy Mn_2CoAl, Appl. Phys. Lett. **113**, 122402 (2018).

[234] Y. Feng, C.-l. Tian, H.-k. Yuan, A.-l. Kuang and H. Chen, Thermodynamic stability, mag-

netism and half metallicity of Mn_2CoAl/GaAs(0 0 1) interface, J. Phys. D: Appl. Phys. **48**, 445003 (2015).

[235] N. Y. Sun, Y. Q. Zhang, H. R. Fu, W. R. Che, C. Y. You, and R. Shan, Perpendicular magnetic anisotropy in Mn_2CoAl thin film, AIP Adv. **6**, 015006 (2016).

[236] Y. Xin, H. Hao, Y.Ma, H. Luo, F. Meng, H. Liu, E. Liu, and G. Wu, Competition of XA and $L2_1B$ ordering in Heusler alloys Mn_2CoZ (Z = Al, Ga, Si, Ge and Sb) and its influence on electronic structure, Intermetallics **80**, 10-15 (2017).

[237] Y. J. Zhang, G. J. Li, E. K. Liu, J. L. Chen, W. H. Wang, and G. H. Wu, Ferromagnetic structures in Mn_2CoGa and Mn_2CoAl doped by Co, Cu, V, and Ti, J. Appl. Phys. **113**, 123901 (2013).

[238] G. Z. Xu, Y. Du, X. M. Zhang, H. G. Zhang, E. K. Liu, W. H. Wang, and G. H. Wu, Magneto-transport properties of oriented Mn_2CoAl films sputtered on thermally oxidized Si substrates, Appl. Phys. Lett. **104**, 242408 (2014).

[239] K. Ueda, S. Hirose, and H. Asano, Ambipolar transport in Mn_2CoAl films by ionic liquid gating, Appl. Phys. Lett. **110**, 202405 (2017).

[240] M. E. Jamer, B. A. Assaf, T. Devakul, and D. Heiman, Magnetic and transport properties of Mn_2CoAl oriented films, Appl. Phys. Lett. **103**, 142403 (2013).

[241] J. Kudrnovský, V. Drchal, and I. Turek, Anomalous Hall effect in stoichiometric Heusler alloys with native disorder: A first-principles study. Phys. Rev. B **88**, 014422 (2013).

[242] B. M. Ludbrook, G. Dubuis, A.-H. Puichaud, B. J. Ruck, and S. Granvill, Nucleation and annihilation of skyrmions in Mn_2CoAl observed through the topological Hall effect. Sci Rep **7**, 13620 (2017).

[243] A. Ullah, B. Balamurugan, W. Zhang, S. Valloppilly, X.-Z. Li, R. Pahari, L.-P. Yue, A. Sokolov, D. J. Sellmyer, and R. Skomski, Crystal Structure and Dzyaloshinski–Moriya Micro-magnetics. IEEE Trans. Magn. **55**, 7100305 (2019).

[244] A. E. Taylor, T. Berlijn, S. E. Hahn, A. F. May, T. J. Williams, L. Poudel, S. Calder, R. S.

Fishman, M. B. Stone, A. A. Aczel, H. B. Cao, M. D. Lumsden, and A. D. Christianson. Influence of interstitial Mn on magnetism in the room-temperature ferromagnet $Mn_{1+\delta}Sb$. Phys. Rev. B **91**, 224418 (2015).